J|A|C|S
ARTICLES

Published on Web 07/31/2009

# On the Mechanism of Lewis Base Catalyzed Aldol Addition Reactions: Kinetic and Spectroscopic Investigations Using Rapid-Injection NMR

Scott E. Denmark,* Brian M. Eklov, Peter J. Yao, and Martin D. Eastgate

*Roger Adams Laboratory, Department of Chemistry, University of Illinois, Urbana, Illinois 61801*

Received April 6, 2009; E-mail: sdenmark@illinois.edu

***Abstract:*** The mechanistic foundations of the Lewis base catalyzed aldol addition reactions have been investigated. From a combination of low-temperature spectroscopic studies ($^{29}$Si and $^{31}$P NMR) and kinetic analyses using a rapid-injection NMR apparatus (RINMR), a correlation of the ground states and transition structures for the aldolization reactions has been formulated. The aldol addition of the *tert*-butylsilyl ketene acetal of *tert*-butyl propanoate with 1-naphthaldehyde is efficiently catalyzed by a combination of silicon tetrachloride and chiral phosphoramide Lewis bases. The rates and selectivities of the aldol additions are highly dependent on the structure of the Lewis bases: bisphosphoramides give the highest rate and selectivity, whereas a related monophosphoramide reacts slowly and with low selectivity. The monophosphoramide shows no nonlinear behavior. All of the additions show a first-order kinetic dependence on silyl ketene acetal and 1-naphthaldehyde and a zeroth-order dependence on silicon tetrachloride. The kinetic order in catalyst is structure dependent and is either half-, two-thirds-, or first-order. All of the phosphoramides are saturated with silicon tetrachloride in some form, and the resting-state species are mixtures of monomeric and dimeric, pentacoordinate cationic, or hexacoordinate neutral complexes. These data allow the formulation of a unified mechanistic scheme based on the postulate of a common reactive intermediate for all catalysts.

## Introduction

The evolution and development of catalytic enantioselective (and diastereoselective) aldol addition reactions represents the apotheosis of organic synthesis methodology. The generality, versatility, and selectivity associated with this process have been thoroughly chronicled in countless books, reviews, and authoritative summaries.[1] Stimulated by the challenges posed by nature, generations of synthetic organic chemists have constructed an impressive edifice of knowledge that constitutes insightful, elegant, and practical solutions to the structural and stereochemical problems presented by polypropionate-derived natural products.[2]

Beyond its obvious utility for the synthesis of natural and non-natural compounds bearing the signature $\beta$-hydroxy carbonyl subunit, the asymmetric aldol addition reaction has been both an engine and a proving ground for new methodological advances. For example, the study of the structure and reactivity of metal enolates,[3] the design and development of chiral Lewis acids based on nearly every element in the periodic table,[4] and the most recent frenzy of disclosures on direct aldolization via enamine catalysis[5] amply illustrate this point. However, despite the enormous impact of these advances for addressing practical problems of efficiency, generality, and selectivity, the extent of fundamental mechanistic understanding of the newly developed processes pales by comparison. Remarkably, the literature in this field is replete with transition structure-based rationalizations for the stereochemical course of these reactions without even the most basic knowledge of the reaction parameters, i.e., the catalyst resting state, the kinetic equation, and the turnover-limiting and stereochemistry-determining steps. Although notable exceptions exist, this situation arises because the advances in analytical chemistry make it much easier to measure

(1) For reviews on catalytic asymmetric aldol reactions, see: (a) *Modern Carbonyl Chemistry*; Otera, J., Ed.; Wiley-VCH: Weinheim, 2000; Chapt. 8. (b) Carreira, E. M. In *Comprehensive Asymmetric Catalysis*; Jacobsen, E. N., Pfaltz, A., Yamamoto, H., Eds.; Springer Verlag: Heidelberg, 1999; Vol. III, Chapt. 29.1. (c) Carreira, E. M.; Fettes, A.; Marti, C. *Org. React.* **2006**, *67*, 1–216. (d) Carreira, E. M. In *Catalytic Asymmetric Synthesis*, 2nd ed.; Ojima, I., Ed.; Wiley-VCH: Weinheim, 2000; Chapt. 8B2. (e) Braun, M. In *Stereoselective Synthesis, Methods of Organic Chemistry (Houben-Weyl)*, Vol. 3, Edition E21; Helmchen, G., Hoffman, R., Mulzer, J., Schaumann, M., Eds.; Thieme: Stuttgart, 1996; p 1603. (f) Nelson, S. G. *Tetrahedron: Asymmetry* **1998**, *9*, 357. (g) For a definitive treatise see: *Modern Aldol Reactions*; Mahrwald, R., Ed.; Wiley-VCH: Weinheim, 2004.

(2) (a) Norcross, R.; Paterson, I. *Chem. Rev.* **1995**, *95*, 2041. (b) Paterson, I.; Cowden, C. J.; Wallace, D. J. In *Modern Carbonyl Chemistry*; Otera, I., Ed.; Wiley-VCH: Weinheim, 2000, Chapt. 9. (c) Florence, G. J.; Gardner, N. M.; Paterson, I. *Nat. Prod. Rep.* **2008**, *25*, 342–375.

(3) (a) Williard, P. G. In *Comprehensive Organic Synthesis, Vol. 1, Additions to C−X Bonds, Part 1*; Trost, B. M., Fleming, I., Eds.; Pergamon: Oxford, 1991; Chapt. 1.1. (b) Seebach, D. *Angew. Chem., Int. Ed. Engl.* **1988**, *27*, 1624–1654. Collum, D. B.; McNeil, A. J.; Ramirez, A. *Angew. Chem., Int. Ed.* **2007**, *46*, 3002–3017.

(4) (a) Yamamoto, H., Ed. *Lewis Acids in Organic Synthesis*; Wiley-VCH: Weinheim, 2000. (b) Santelli, M.; Pons, J.-M. *Lewis Acids and Selectivity in Organic Synthesis*; CRC Press: Boca Raton, FL, 1996.

(5) (a) Berkessel, A.; Groger, H. *Asymmetric Organocatalysis*; Wiley-VCH: Weinheim, 2005. (b) Dalko, P. I.; Moisan, L. *Angew. Chem., Int. Ed.* **2004**, *43*, 5138. (c) Mukherjee, S.; Yang, J. W.; Hoffmann, S.; List, B. *Chem. Rev.* **2007**, *107*, 5471.



**10.1021/ja902474j CCC: $40.75** 

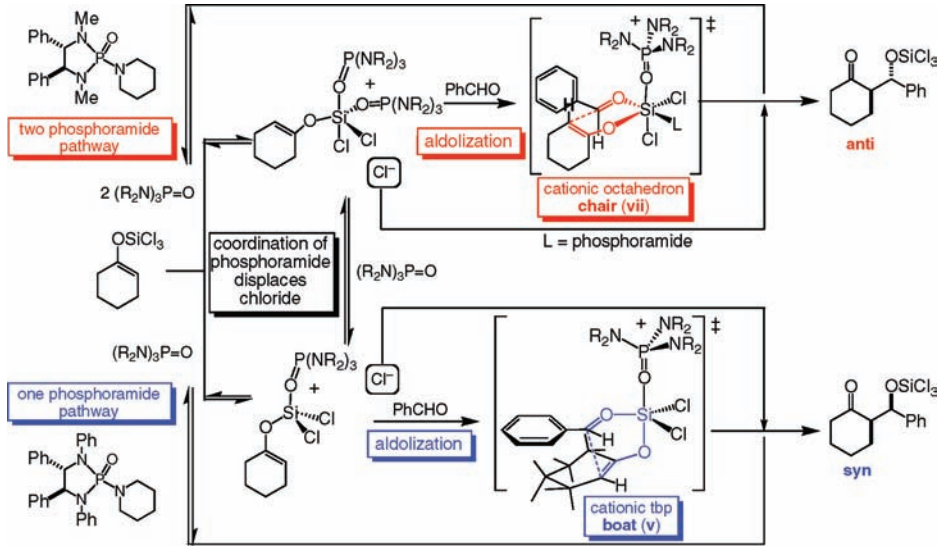


***Figure 1.*** Grand unified mechanistic scheme for phosphoramide-catalyzed aldolization.

an enantiomer ratio or diastereomer ratio than to determine a rate equation.

Commencing in 1996,[6] investigations in these laboratories sought to introduce a new paradigm for catalysis of aldol additions by harnessing the concept of "Lewis base activation of Lewis acids". In the intervening years, the theoretical foundations, methodological development, and generality of this concept have been extensively documented, primarily as illustrated in manifold applications of aldolization reactions.[7] This report discloses our efforts to shed light on the origin of the remarkable catalytic effect of Lewis base activated Lewis acids by laying a concrete mechanistic foundation. We describe herein: (1) spectroscopic studies on the interaction of the Lewis bases (phosphoramides) with the weak Lewis acid, silicon tetrachloride, (2) establishment of the resting states of the adducts, and (3) the full kinetic analysis of the catalytic reactions. These studies have allowed the formulation of a unified theory of catalysis that has implications beyond the aldol addition reaction.

## Background

**1. Summary of Catalytic Enantioselective Aldolization with Chiral Lewis Bases. 1.1. Enoxytrichlorosilanes.** The original incarnation of the Lewis base catalyzed aldol addition reaction involved the use of preformed trichlorosilyl enolates of esters,[6,8] ketones,[9] and aldehydes.[10] These reagents undergo high-yielding and selective additions to both aldehydes and ketones under catalysis by Lewis bases, primarily chiral phosphoramides or N-oxides. In addition to a thorough exploration of reaction scope, extensive mechanistic investigations[11] revealed the following generalizations: (1) the reaction displays first-order dependence on enoxytrichlorosilane and aldehyde, and first- or second-order dependence on catalyst, (2) the addition takes place via the simultaneous operation of two mechanistic pathways involving either one or two phosphoramides bound to a pentacoordinate siliconium ion organizational center, (3) the aldol addition occurs through the reversible albeit unfavorable formation of an activated complex, and (4) the turnover-limiting and stereodetermining step is the aldol addition. Finally, the effects of catalyst loading, rate of addition, solvents, and additives have been studied and together allow the formulation of a unified mechanistic picture for the aldol addition, Figure 1.

**1.2. Enoxytrialkylsilanes.** In recent years, all of the methodological efforts in this area have focused on the use of Lewis base activated Lewis acids to effect highly general and selective Mukaiyama-type directed aldol additions[12] of enoxysilane derivatives of esters,[13] nitriles,[14] ketones,[9a,15] aldehydes,[16] unsaturated esters,[17] ketones, and amides.[18] All of these reactions

(6) Denmark, S. E.; Winter, S. B. D.; Su, X.; Wong, K.-T. *J. Am. Chem. Soc.* **1996**, *118*, 7404–7405.
(7) (a) Denmark, S. E.; Beutner, G. L. *Angew. Chem., Int. Ed.* **2008**, *47*, 1560–1638. (b) Denmark, S. E.; Fujimori, S. In *Modern Aldol Reactions*; Mahrwald, R., Ed.; Wiley-VCH: Weinheim, 2004; Vol. 2, Chapt. 7. (c) Denmark, S. E.; Stavenger, R. A. *Acc. Chem. Res.* **2000**, *33*, 432.
(8) (a) Denmark, S. E.; Fan, Y. *J. Am. Chem. Soc.* **2002**, *124*, 4233–4235. (b) Denmark, S. E.; Fan, Y.; Eastgate, M. D. *J. Org. Chem.* **2005**, *70*, 5235–5248.
(9) (a) Denmark, S. E.; Fujimori, S.; Pham, S. M. *J. Org. Chem.* **2005**, *70*, 10823–10840. (b) Denmark, S. E.; Pham, S. M. *J. Org. Chem.* **2003**, *68*, 5045–5055. (c) Denmark, S. E.; Stavenger, R. A.; Wong, K.-T.; Su, X. *J. Am. Chem. Soc.* **1999**, *121*, 4982–4991. (d) Denmark, S. E.; Stavenger, R. A. *J. Am. Chem. Soc.* **2000**, *122*, 8837–8847. (e) Denmark, S. E.; Stavenger, R. A.; Wong, K.-T. *Tetrahedron* **1998**, *54*, 10389–10402. (f) Denmark, S. E.; Su, X.; Nishigaichi, Y. *J. Am. Chem. Soc.* **1998**, *120*, 12990–12991.
(10) (a) Denmark, S. E.; Ghosh, S. K. *Tetrahedron* **2007**, *63*, 8636–8644. (b) Denmark, S. E.; Bui, T. *Proc. Natl. Acad. Sci. U.S.A.* **2004**, *101*, 5439–5444. (c) Denmark, S. E.; Ghosh, S. K. *Angew. Chem., Int. Ed.* **2001**, *40*, 4759–4762.
(11) (a) Denmark, S. E.; Pham, S. M.; Stavenger, R. A.; Su, X.; Wong, K.-T.; Nishigaichi, Y. *J. Org. Chem.* **2006**, *71*, 3904–3022. (b) Denmark, S. E.; Bui, T. *J. Org. Chem.* **2005**, *70*, 10393–10399. (c) Denmark, S. E.; Pham, S. M. *Helv. Chim. Acta* **2000**, *83*, 1846–1853. (d) Denmark, S. E.; Su, X. *Tetrahedron* **1999**, *55*, 8727–8738.
(12) (a) Mukaiyama, T. *Org. React.* **1982**, *28*, 203–331. (b) Mukaiyama, T.; Kobayashi, S. *Org. React.* **1994**, *46*, 1–103. (c) Mukaiyama, T.; Matsuo, T. In *Modern Aldol Reactions*; Mahrwald, R., Ed.; Wiley-VCH: Weinheim, 2004; Vol. 1, Chapt. 3.
(13) (a) Denmark, S. E.; Beutner, G. L.; Wynn, T.; Eastgate, M. D. *J. Am. Chem. Soc.* **2005**, *127*, 3774–3789. (b) Denmark, S. E.; Chung, W.-j. *J. Org. Chem.* **2008**, *73*, 4582–4595.
(14) Denmark, S. E.; Wilson, T. W.; Burk, M. T.; Heemstra, J. R., Jr. *J. Am. Chem. Soc.* **2007**, *129*, 14864–14865.
(15) Denmark, S. E.; Heemstra, J. R., Jr. *Org. Lett.* **2003**, *5*, 2303–2306.
(16) Denmark, S. E.; Bui, T. *J. Org. Chem.* **2005**, *70*, 10190–10193.
(17) Denmark, S. E.; Beutner, G. L. *J. Am. Chem. Soc.* **2003**, *125*, 7800–7801.
(18) Denmark, S. E.; Heemstra, J. R., Jr. *J. Org. Chem.* **2007**, *72*, 5668–5688.

share a common pathway in which an in situ-generated chiral Lewis acid catalyzes the addition of one of the above-mentioned nucleophiles to a range of aldehydes. The conceptual basis for the activation of the nascent Lewis acid (silicon tetrachloride) derives from the rehybridization of the Lewis acid−base adduct, Scheme 1, and has been discussed in detail elsewhere.[7a] During the development of the various aldol additions catalyzed by this unique Lewis acid, a working hypothesis for the mechanism of the process was formulated that borrowed heavily from our understanding of the cognate reactions of enoxytrichlorosilanes described above. However, from simple empirical analysis of the rates, selectivities, substrate scope, and response to experimental variables, it was clear that the two manifolds were not completely congruent. In addition, no definitive mechanistic studies supported the validity of those analogies. Accordingly, we undertook the challenge of placing this newer family of catalyzed aldol additions on the same concrete foundation that now exists for the enoxytrichlorosilane additions.

***Scheme 1***

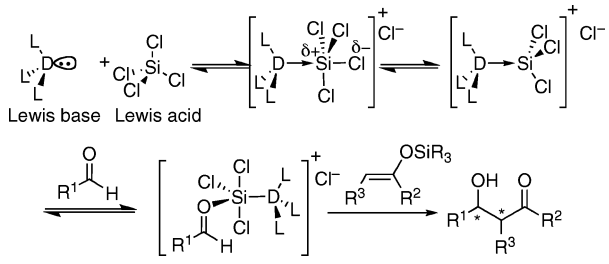


**2. Objectives of This Study.** To investigate the validity of the working hypothesis outlined in Scheme 1, the following reaction parameters needed clarification: (1) the effect on reaction rate and enantioselectivity of different catalyst structures, (2) the molecularity of the transition structure, (3) the stoichiometry, structure, and equilibrium position of the Lewis base−Lewis acid association, and (4) the overall rate equation and partial orders with respect to all reaction components. Ultimately, our goal was to formulate a unified mechanistic picture that could explain the origin of catalysis and selectivity. We describe herein the successful realization of the first of these two highly ambitious goals. The second, i.e., rationalization of selectivity, will require extensive computational analysis of the structures that have been established in this study.

**3. Challenges and Solutions: Development and Implementation of RINMR Spectroscopic Analysis.** Monitoring the progress of a dilute (ca. 40 mM) reaction that has a half-life of less than 90 s at −78 °C is a daunting task. Only spectroscopic methods are viable at these temperatures.[19] Although IR spectroscopy is popular for reaction monitoring, at concentrations below 0.1 M, the low sensitivity of this technique is prohibitive. Monitoring the progress of these reactions by NMR spectroscopy is ideal as it allows exquisite sensitivity, the ability to operate over a wide range of temperatures, and the observation of any well-resolved resonance(s), whether correlated to starting material, intermediate, or product.

The difficulty in this case is rapidly delivering a known amount of a temperature-equilibrated reagent into a temperature-equilibrated substrate while the sample is spinning in the NMR spectrometer and ready for acquisition, all while coordinating the injection event with data acquisition. Care must then be taken to ensure that the data are collected in a manner that produces integral values that are not only internally consistent (resonance to resonance within a single spectrum) but also consistent among the plethora of spectra collected over the course of an individual experiment. To this end, we have developed a rapid-injection system that, when coupled with a high-sensitivity $^1$H NMR probe,[20] allows us to accurately inject a known volume of a reagent solution into a sample tube inside the magnet (and controlled by the spectrometer console), even while the tube is spinning at −78 °C.[21]

This system allows reactions to be monitored under conditions that are identical to, or very closely resemble, those employed in the preparative system, minimizing the danger that the results will not be representative of those from preparative reactions. In our case, four minor adjustments were made to the preparative system to allow the reactions of interest to be studied reproducibly: (1) the overall concentration (0.076 M) was dropped to one-third that of the preparative conditions, (2) chromium(III) tris(dipivaloylmethane)[22] [Cr(dpm)$_3$, 5 mM] was added as a paramagnetic relaxation agent to allow a more rapid acquisition cycle while ensuring integral accuracy, (3) the injected reagent was dissolved in $CDCl_3$, not $CD_2Cl_2$, and (4) the reactions were performed at −60 °C. For these studies, 1-naphthaldehyde was chosen as the aldehyde component due to the exquisite selectivities observed with this substrate, as well as its lower rate of reaction.

Employing this system to study the asymmetric Lewis base catalyzed aldol reaction allowed us to study the reaction under the preparative conditions. That is, each sample tube can be filled with all of the reagents (1-naphthaldehyde,[23] $SiCl_4$, DIPEA, and the Lewis basic catalyst) dissolved in $CD_2Cl_2$ with added Cr(dpm)$_3$, Scheme 2. All concentrations but one were held constant, while the concentration of the reagent being studied was varied from 0.25, 0.5, 1, and 2 times the normal reaction concentration (for an 8-fold range). All of the samples were stored under an inert atmosphere at −78 °C, before being placed into the precooled (−60 °C) spectrometer. Once the sample was in the magnet, the injector was inserted into the sample tube while it was spinning, and the entire apparatus was temperature equilibrated for a period of 5−10 min, which allowed the sample in the injector to cool. A vigorous flow of nitrogen (between 10 and 20 L/min) through the probe was maintained to ensure rapid equilibration. The magnetic field was shimmed in the normal fashion, the spectrometer was pro-

(19) Reaction calorimetry at this temperature is challenging and lacks reproducibility, and ex situ analysis of a quenched aliquot requires that no significant warming of the sample occur before the quench, a very difficult task in this temperature regime.

(20) The temperature range is determined by the conditions that the probe can support. The Varian 10 mm broadband probe used in these studies has operating limits of −130 and +100 °C.

(21) The details of the design, implementation, calibration, and use of this system are not the subject of this publication and will be published in due course. For descriptions and results from pioneering RINMR studies, see: (a) McGarrity, J. F.; Prodolliet, J.; Smyth, T. *Org. Magn. Reson.* **1981**, *17*, 59. (b) Palmer, C. A.; Ogle, C. A.; Arnett, E. M. *J. Am. Chem. Soc.* **1992**, *114*, 5619. (c) Reetz, M. T.; Raguse, B.; Marth, C. F.; Hügel, H. M.; Bach, T.; Fox, D. N. A. *Tetrahedron* **1992**, *48*, 5731.

(22) The additive Cr(dpm)$_3$ was chosen over the more popular Cr(acac)$_3$ due to its decreased Lewis acidity, minimizing the chance that it would interfere with the reaction. Control experiments showed no measurable influence of this additive on the rate of reaction, as well as no reactivity in the absence of $SiCl_4$ (see Supporting Information). Levy, G. C.; Edlund, U.; Hexem, J. G. *J. Magn. Reson.* **1975**, *19*, 259–262.

(23) Commercial 1-naphthaldehyde is contaminated with ca. 10% 2-naphthaldehyde, which reacts faster than 1-naphthaldehyde. The 1-naphthaldehyde used in these kinetic studies was purified to ≥99.8% purity before use. Details are in the Supporting Information.

grammed to automate the injection of a precisely known amount of the precooled solution of the silyl ketene acetal, and the sequence was started. After the spectrometer collected five spectra without the silyl ketene acetal, the spectrometer would trigger the injection event and resume acquiring data at set intervals (in this case, 3-s intervals). Typically, 0.200 mL of the silyl ketene acetal solution was injected into a 3.0 mL sample.

***Scheme 2***

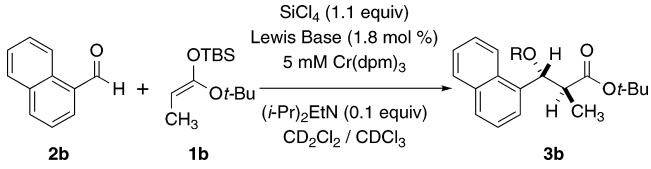


Figure 2 shows an excerpt of the $^1$H NMR data obtained from a typical run. The aldehyde (initial concentration, 39 mM) displays two resonances ($\delta = 9.3$ and 10.3 ppm) that are well-resolved and that allow the concentration change in this starting material to be easily monitored. Similarly, a resonance corresponding to the product aldolate can be observed ($\delta = 6.2$ ppm). Orienting experiments demonstrated that the concentration decrease displayed by both the aldehyde and silyl ketene acetal directly led to a corresponding increase in the aldolate; no intermediate species were observed. In practice, the disappearance of 1-naphthaldehyde was routinely monitored.

A great deal of mechanical and electrical optimization of the injection system was performed during its design and initial testing to ensure reproducibility and accuracy of the obtained data. Although some of these details have been reported,[11c] a full account will be published in a more suitable venue. Optimization of the NMR parameters themselves is critical to the collection of reproducibly accurate integral data and must be discussed in some detail.

The techniques necessary to collect quantitative NMR data are well-known and well-developed.[24] The two main factors that require our attention are magnetization recovery and appropriate signal collection, both of which are related to the $T_1$ relaxation times of the samples.

Optimization of the data collection began by determining the 90° pulse (pw90) for a sample at ca. 50% conversion so that all species, including the product, were observable in solution. The optimized pw90 value was determined to be 30 $\mu$s with a transmitter power of 60 db. A $T_1$ determination by inversion recovery showed that this sample's longest $T_1$ value was displayed by the aldehyde proton and was on the order of 3 s. Consequently, the relaxation delay (d1) was set to 15 s minus the acquisition time (at; d1 = 15 − at), to allow 5 times the measured $T_1$ between pulses. Unfortunately, these conditions did not allow data collection to occur rapidly enough to obtain good initial reaction rate data. Even at −60 °C, the reaction progressed too quickly to be monitored under these conditions.

Next, methods to shorten the time between pulses were implemented. Decreasing the pulse width from 90° to 45° would allow one pulse every 12 rather than every 15 s, a rather insignificant change. Reducing the pulse width further would begin to severely impact the resulting signal-to-noise and was not considered. Ultimately, the addition of a paramagnetic relaxation agent, chromium(III) dipivaloylmethane [Cr(dpm)$_3$], gave the desired results.[25] Like its congener Cr(acac)$_3$, Cr(dpm)$_3$ reduces $T_1$ times, but it is less Lewis acidic than Cr(acac)$_3$ because of the increased steric bulk about the central chromium atom.

The optimal concentration of Cr(dpm)$_3$ was briefly investigated. As discussed above, in the absence of Cr(dpm)$_3$, the longest $T_1$ was 3 s, requiring 15 s between pulses. At 1 mM in Cr(dpm)$_3$, the longest $T_1$ dropped to 1.4 s, requiring 7 s between pulses. At 5 mM in Cr(dpm)$_3$, the longest $T_1$ was 0.5 s, requiring 2.5 s between pulses. We decided to use 5 mM Cr(dpm)$_3$ and a total time between pulses of 3 s. A control experiment with 5 mM Cr(dpm)$_3$ but without SiCl$_4$ showed no consumption of either the aldehyde or silyl ketene acetal over 20 min at −60 °C. A typical SiCl$_4$-catalyzed reaction was complete within this

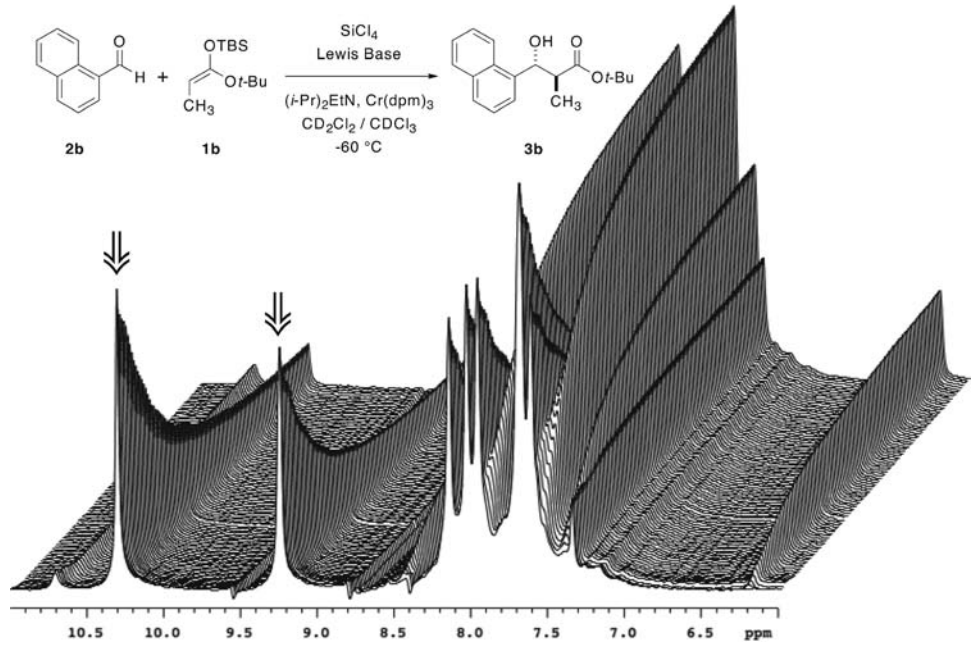


***Figure 2.*** A portion of the NMR spectral data collected over the course of 900 s. Data were collected every 3 s, but only every third spectrum (every 9 s) is shown here for clarity. The disappearance of 1-naphthaldehyde is clear ($\delta = 9.25$ and 10.3 ppm), as is the appearance of the product aldolate ($\delta = 6.2$ ppm).

time frame. This observation, combined with the similarities in observed rates of reaction with and without the added $Cr(dpm)_3$, provides convincing evidence that the relaxation agent does not affect the outcome or rate of the reaction. In practice, a 3-s data acquisition without a relaxation delay between pulses was employed. This setup provides 6 times the longest $T_1$ value between pulses and also ensures that all of the available signal has been collected. These parameters allowed the collection of very reproducible data sets and were used throughout the study.

After data collection was complete, integral regions were cut to include 5 times the line width, and an automated routine was employed to tabulate the integral data from all of the spectra collected (measurements were made on 3-s intervals until 20% conversion or, for slow reactions, 1200 s).

When combined, the addition of the relaxation agent, the optimized data collection, and integral determination routines allowed the collection of exquisitely reproducible data sets.

## Results

**1. Enantioselective Aldol Additions.** The reactions studied in this work are the enantio- and diastereoselective aldol addition reactions between silyl ketene acetals (**1a/1b**) and benzaldehyde (**2a**) or 1-naphthaldehyde (**2b**), Scheme 3. The aldol additions of both acetate- and propanoate-derived silyl ketene acetals were studied with the two different aldehydes to demonstrate the generality of the trends observed in phosphoramide structure. The full kinetic analysis was carried out only for the reactions of **1b** and **2b**. Several phosphoramides were used as catalysts: hexamethylphosphoric triamide (HMPA), the monophosphoramide **5**, and the bisphosphoramides **4a**−**4d** wherein the chain length between the phosphoramides varied from 3 to 6 methylene units. The results of the catalyst dependence are collected in Table 1.

The addition of **1a** to **2a** was examined with four different catalysts (Table 1, entries 1−4). Each phosphoramide catalyzed the reaction in high yield (89−94%) but with only a modest effect of catalyst structure on enantioselectivity. These selectivities closely matched those obtained previously for the addition of allyltributylstannane to benzaldehyde with $SiCl_4$.[26] Similarly, the addition of **1b** to **2b** proceeded in good yield and with high anti diastereoselectivity, despite the use of a 9:1 mixture of (*E*)-**2**/(*Z*)-**2**. Although we knew that the reaction catalyzed by **4c** was extremely fast, we did not know the rates of the reactions catalyzed by the other phosphoramides; consequently, all the reactions were run at −78 °C for 3 h. Interestingly, the enantioselectivities were significantly more sensitive to the tether length. As has always been observed, **4c** ($n = 5$) gave the highest enantioselectivity (97:3). Bisphosphoramides with shorter chain lengths (**4a** and **4b**) showed moderately lower selectivities (93:7 and 84:16), while the catalyst with a longer chain length (**4d**) and monophosphoramide **5** showed significantly lower selectivities (72:28 and 77:23). The greater sensitivity of the **1b/2b** combination to changes in catalyst structure suggested that the full kinetic analysis of this system would likely be more informative.

**2. Nonlinear Effect Studies.** In previous mechanistic studies of Lewis base catalyzed reactions (aldol additions of trichlorosilyl enolates,[11] allylation with allyltrichlorosilanes,[27] and epoxide ring-opening with silicon tetrachloride[28]), important insights on the nature of phosphoramide·Si interaction were secured by carrying out nonlinear effect studies.[29] Thus, to glean as much information from this process as possible, a nonlinear effect study was undertaken for the addition of **1a** to **2a**.

Both (*R*)-**5** and (*S*)-**5** were independently prepared by the previously described method and were assured to be of >99.9% enantiopurity by CSP-SFC analysis.[30] The enantiopure catalysts were then combined in nominal ratios to provide enantiomeric mixtures (60:40, 70:30, 80:20, and 90:10) for the nonlinear study, and the enantiomeric ratios were independently confirmed by SFC analysis (59.3:40.7, 68.8:31.2, 78.3:21.6, 88.9:11.1).

The aldol addition was then carried out as described above, and the enantiopurity of the aldol product was determined by CSP-SFC analysis. The reactions were carried out in triplicate (yields all >90%), and each product was analyzed three times. When the averaged results are represented graphically, ee of

***Scheme 3***

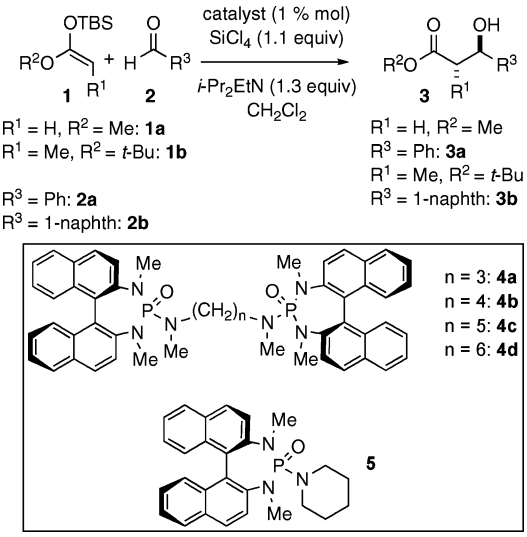


***Table 1.*** Catalyzed Additions of **1** to **2** with Chiral Lewis Bases (Scheme 3)

| entry | ketene acetal | catalyst (mol %) | time, h | product | temp, °C | yield, % | er |
|---|---|---|---|---|---|---|---|
| 1 | **1a** | **5** (5.0) | 1 | **3a** | −78 | 94 | 89:11 |
| 2 | **1a** | **4b** (2.5) | 1 | **3a** | −78 | 92 | 91:9 |
| 3 | **1a** | **4c** (5.0) | 1 | **3a** | −78 | 97 | 96:4[a] |
| 4 | **1a** | **4d** (2.5) | 1 | **3a** | −78 | 90 | 88:12 |
| 5 | **1b** | HMPA | | **3b** | | | |
| 6 | **1b** | **5** (1.0) | 3 | **3b** | −78 | 80 | 77:23 |
| 7 | **1b** | **4a** (1.0) | 3 | **3b** | −78 | 77 | 93:7 |
| 8 | **1b** | **4b** (1.0) | 3 | **3b** | −78 | 83 | 84:16 |
| 9 | **1b** | **4c** (1.0) | 3 | **3b** | −78 | 98 | 97:3[a] |
| 10 | **1b** | **4d** (1.0) | 3 | **3b** | −78 | 78 | 72:28 |

[a] Data taken from ref 13a.

(24) For example, see: (a) Gerritz, S. W.; Sefler, A. M. *J. Comb. Chem.* **2000**, *2*, 39–41. (b) Hoye, T. R.; Eklov, B. M.; Voloshin, M. *Org. Lett.* **2004**, *6*, 2567–2570.
(25) Stille, D.; Doyle, J. R. *Inorg. Synth.* **1986**, *24*, 183–184.
(26) Denmark, S. E.; Wynn, T. *J. Am. Chem. Soc.* **2001**, *123*, 6199–6200.
(27) Denmark, S. E.; Fu, J.; Coe, D. M.; Su, X.; Pratt, N. E.; Griedel, B. D. *J. Org. Chem.* **2006**, *71*, 1513–1522.
(28) Denmark, S. E.; Barsanti, P. A.; Beutner, G. L.; Wilson, T. W. *Adv. Synth. Catal.* **2007**, *349*, 567–582.
(29) (a) Guillaneux, D.; Zhao, S.-H.; Samuel, O.; Rainford, D.; Kagan, H. B. *J. Am. Chem. Soc.* **1994**, *116*, 9430–9439. (b) Fenwick, D. R.; Kagan, H. B. *Top. Stereochem.* **1999**, *22*, 257–296. (c) Girard, G. L.; Kagan, H. B. *Angew. Chem., Int. Ed.* **1998**, *37*, 2923–2959. (d) Avalos, M.; Babiano, R.; Cintas, P.; Jimenez, J. L.; Palacios, J. C. *Tetrahedron: Asymmetry* **1997**, *8*, 2997–3017.
(30) Denmark, S. E.; Su, X.; Nishigaichi, Y.; Coe, D. M.; Wong, K.-T. *J. Org. Chem.* **1999**, *64*, 1958.

the catalyst vs ee of the product, a linear relationship is clearly observed, Figure 3.

The absence of a nonlinear effect is surprising given that an effect has been seen in all previous studies. In light of the full kinetic studies described below, the implications of this outcome will be deferred to the Discussion section.

**3. RINMR Kinetic Analysis of the Addition of 1b to 2b.**

**3.1. Partial Order in Each Reagent with Catalyst 4c.** Optimization of the NMR parameters occurred before beginning to measure rates of reactions and was discussed above. It was decided early on to monitor the disappearance of aldehyde, as the two well-resolved resonances at $\delta = 9.3$ and 10.3 ppm could be monitored and averaged to measure the changes in concentration for each run.

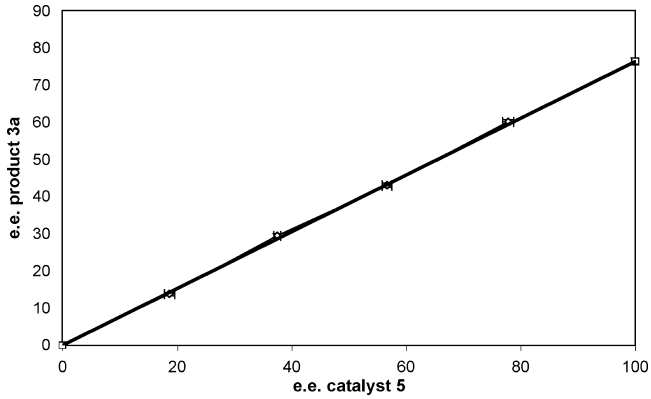


***Figure 3.*** Nonlinear effect study of acetate aldolization with catalyst **5**.

The partial reaction order of each reagent was determined by the initial rates method. The concentration of each individual reactant was varied over an 8-fold range, while holding all other reagent concentrations constant and observing the changes in concentration over the first 5−20% conversion. As shown in Figure 4, both silyl ketene acetal **1b** (12, 24, 48, and 96 mM) and 1-naphthaldehyde (**2b**) (9.2, 20, 39, and 78 mM) displayed first-order behaviors. The reaction orders for silicon tetrachloride and the bisphosphoramide catalyst **4c** were more surprising. Varying the concentration of silicon tetrachloride (44, 87, 174, and 348 mM) had no effect upon the rate of the reaction, while the partial reaction order in **4c** (0.18, 0.36, 0.72, and 1.43 mM) was 0.5, Figure 5. Taken together, these two results provide the greatest insight into the structure of the catalyst resting state and the active catalytic species. However, the complete picture still requires the analysis of the other catalysts, as described below.

Although not contributors to the stoichiometric process, the partial orders in all of the other reaction components were also obtained. Varying the concentration of diisopropylethylamine (added as an acid scavenger) and $Cr(dpm_3)$ (the added paramagnetic relaxation agent) had no effect upon the rate of reaction. Interestingly, varying the concentration of chloride by the addition of tetrabutylammonium chloride (4, 8,16, and 32 mM) gave rise to a negative fractional order (−0.2), whereas the addition of tetrabutylammonium triflate (4, 8, 16, and 32 mM) did not affect the rate of reaction.

**3.2. Partial Order in Catalysts. 3.2.1. HMPA.** Because the complexation behavior of HMPA and $SiCl_4$ has been studied in depth,[31] and HMPA is known to be an active, albeit sluggish

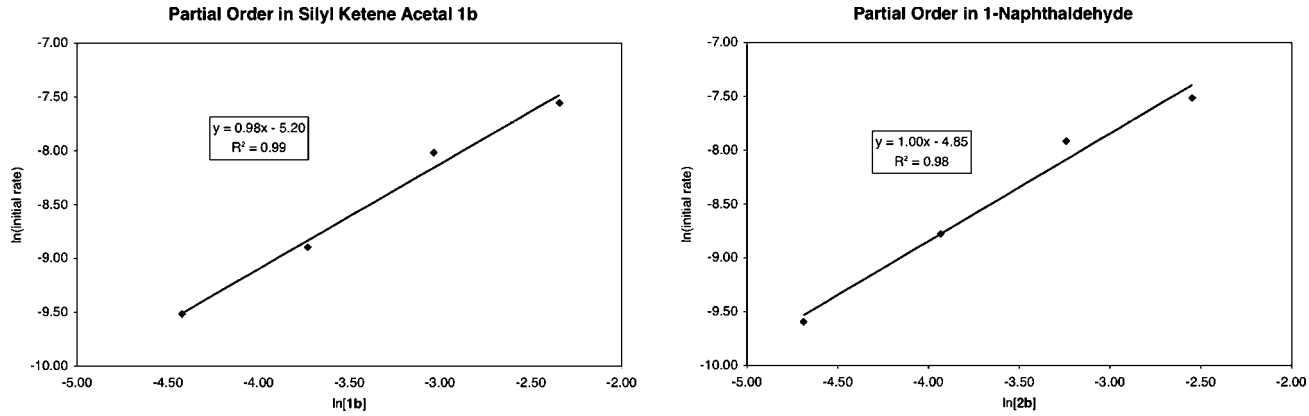


***Figure 4.*** Partial reaction order in silyl ketene acetal **1b** and 1-naphthaldehdye (**2b**).

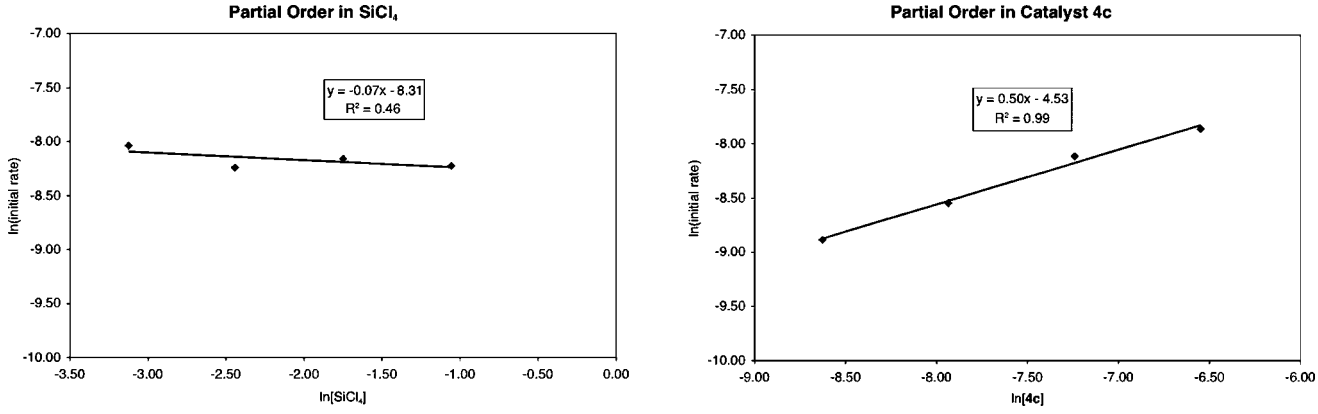


***Figure 5.*** Partial reaction order in $SiCl_4$ and **4c**.

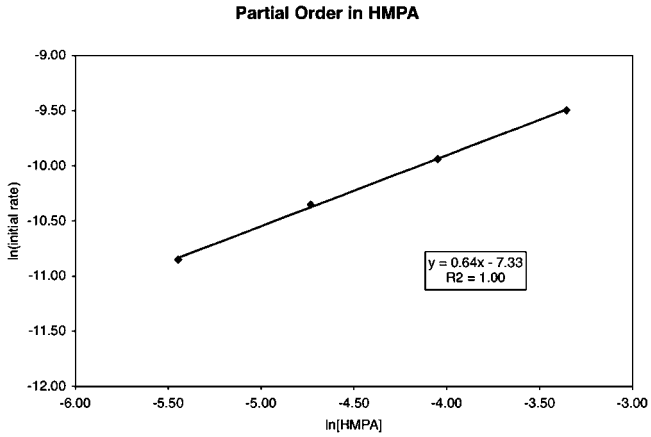


***Figure 6.*** Partial reaction order in HMPA.

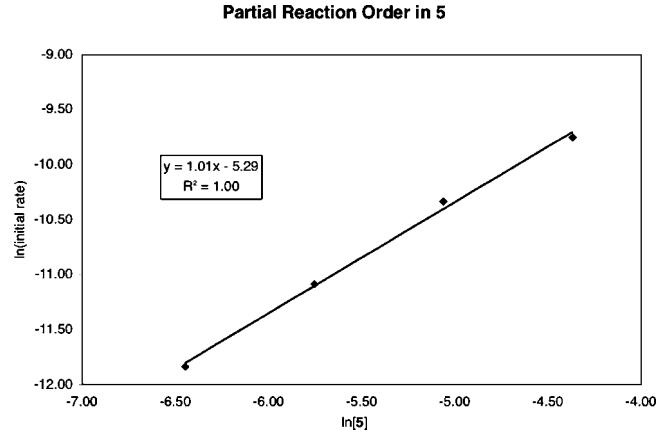


***Figure 7.*** Partial reaction order in monophosphoramide **5**.

catalyst for this aldol reaction, learning how varying its concentration affects the rate of reaction would be instructive. Indeed, following the analysis above, HMPA (4, 9, 17, and 35 mM) displayed an interesting fractional order dependence (0.64), Figure 6. This result was most certainly not expected. If the working hypothesis for the catalytic cycle outlined above was correct, HMPA should have displayed a second-order behavior. The approximate two-thirds order is intriguing and will be discussed below.

**3.2.2. Monophosphoramide 5.** Although catalyst **5** afforded low enantioselectivities in the aldol additions, it is nonetheless of mechanistic interest. In previous studies of the reactions of enoxytrichlorosilanes and allyltrichlorosilanes, two independent mechanistic pathways involving one and two phosphoramides could be discerned. The latter, higher order pathway afforded greater rates and selectivities (which stimulated the development of the bisphosphoramides). Surprisingly, this catalyst displayed a first-order dependence when its concentration was varied (1.6, 3.2, 6.3, and 12.7 mM, Figure 7). As was the case with HMPA, this result is an interesting departure from the expected second-order behavior. Any proposal for a catalytic cycle will have to explain why each of the catalysts discussed so far displays different partial reaction orders.

**3.2.3. Bisphosphoramide Catalysts 4a, 4b, and 4d.** As noted previously, catalyst **4c**, with a five-methylene chain length, showed 0.5 partial reaction order. Increasing the chain length to six methylenes gave the same 0.5 partial reaction order for catalyst **4d**, Figure 8, with similar initial rates. Unexpectedly, by decreasing the chain length to three and four methylenes (**4a** and **4b**), the partial reaction order changed to unity! These catalysts also showed remarkably faster initial rates than **4c** and **4d**. In fact, for catalyst **4a** the initial rates were almost too fast for the kinetic studies (50% conversion in 300 s with 0.08 mol % **4a**), and some caution must be exercised in interpreting the results for this catalyst. Catalyst **4b** showed slightly slower initial rates (but still much faster than **4c** and **4d**), and its results can be interpreted with a much higher degree of confidence. It should be noted that the partial orders in **1b**, 1-naphthaldehyde, $SiCl_4$, diisopropylethylamine, and $Cr(dpm)_3$ were obtained with catalyst **4c** only. It is assumed that the orders in these reagents are preserved across the entire series of catalysts.

**4. Catalyst Resting State.** The interpretation of the rate data presented above is intimately tied to the identity of the catalyst resting state. Thus, to provide insight into the structure and composition of the species formed by combining the phosphoramides with $SiCl_4$, a series of $^{29}Si$ and $^{31}P$ NMR spectroscopic experiments were performed with mixtures of each of the catalysts **4a**−**4d** and **5** together with $SiCl_4$. The species detected under these conditions are not rigorously the catalyst resting states because no catalytic process is operating. However, the rate and concentration of the catalytic reactions preclude any chance of obtaining information at natural abundance of $^{29}Si$. Thus, all conclusions drawn from these studies must be tempered with that caveat. Nevertheless, very useful information could be gathered that merits presentation and analysis.

NMR spectra recorded at room temperature showed that the species observed in all of these mixtures were fluxional. When the spectra were recorded between −70 and −100 °C, sharp, well-resolved signals could be observed. Again, $Cr(dpm)_3$ was added to the samples to reduce the long $^{29}Si$ $T_1$ times. Silicon-29 chemical shifts are highly dependent on coordination number and fall into three major regions—four coordinate (+10 to −30 ppm), five coordinate (−50 to −120 ppm), and six coordinate (−150 to −200 ppm); thus, Si-29 spectra are ideally suited for the analysis of the possible coordinate structures of the $SiCl_4$ catalyst.[32]

**4.1. HMPA/$SiCl_4$.** Previous investigations of the $SiCl_4$/HMPA system have shown that even when HMPA is present in substoichiometric amounts, three major species are present in solution, Figure 9: a cationic, five-coordinate complex, [*trans*-$HMPA_2 \cdot SiCl_3]^+Cl^-$ (−120.5 ppm, $J$ = 15 Hz),[33] and two six-coordinate complexes, one cationic, [*mer*-$HMPA_3SiCl_3]^+Cl^-$ (−206 ppm, s), and one neutral, [*trans*-$HMPA_2 \cdot SiCl_4$] (−207.8, s), Scheme 4.[31] This observation reveals the strong thermodynamic preference for the formation of these complexes. In fact, no free HMPA was observed in solution until more than 3.0 equiv of HMPA had been added.[34] Moreover, no species with a single bound phosphoramide was identified; all of the species observed in solution had either two or three phosphoramides bound to a central silicon atom.

(31) Denmark, S. E.; Eklov, B. M. *Chem. Eur. J.* **2008**, *14*, 234–239.

(32) (a) Kennedy, J. D.; McFarlane, W. In *Multinuclear NMR*; Mason, J., Ed.; Plenum Press: New York, 1987; Chapt. 11. (b) Kobayashi, S.; Nishio, K. *Tetrahedron Lett.* **1993**, *34*, 3453. (c) Olsson, L.; Ottosson, C. H.; Cremer, D. *J. Am. Chem. Soc.* **1995**, *117*, 7460. (d) Arshadi, M.; Johnels, D.; Edlund, U.; Ottoson, C.-H.; Cremer, D. *J. Am. Chem. Soc.* **1996**, *118*, 5120.

(33) In our earlier publication,[31] this resonance was erroneously assigned to be the cis complex, which is inconsistent with the 15 Hz coupling constant.

(34) Conversely, free $SiCl_4$ was always observed in the $^{29}Si$ NMR spectrum until 3.0 equiv of HMPA had been added.

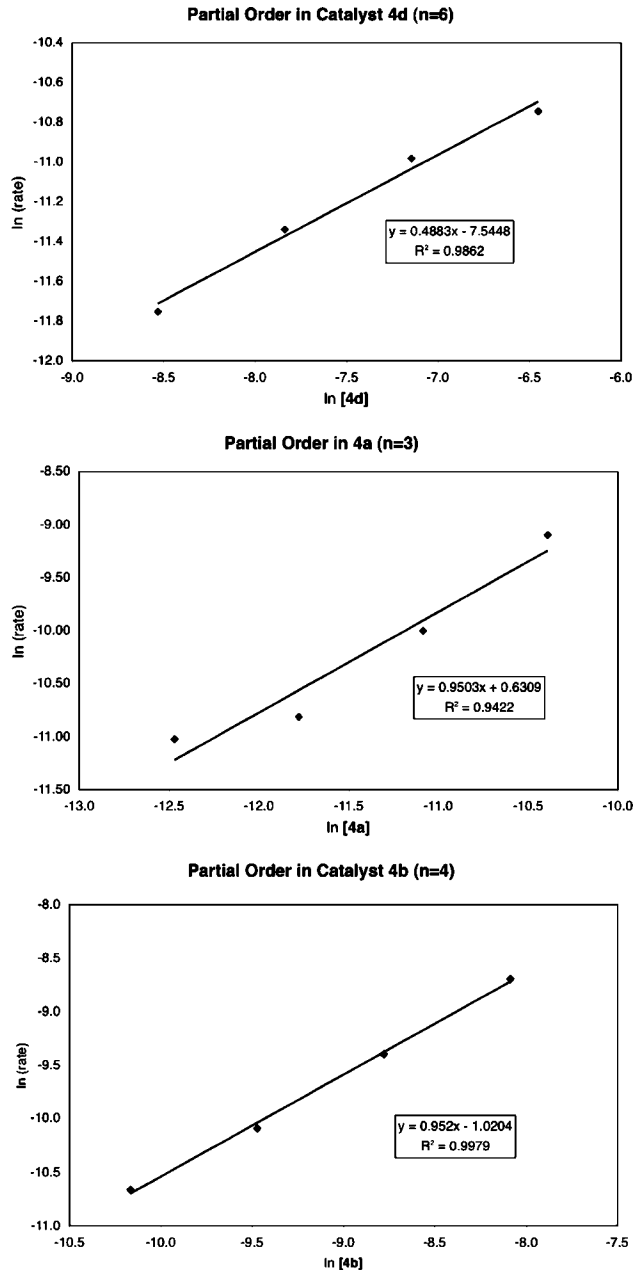


***Figure 8.*** Partial reaction order in bisphosphoramides **4d**, **4a**, and **4b**.

***Scheme 4***

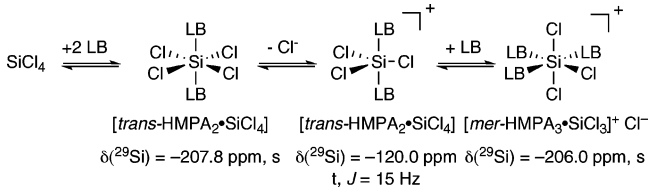


**4.2. Monophosphoramide 5/$SiCl_4$.** The $^{29}Si$ NMR spectroscopic analysis of a 4:1 mixture of $SiCl_4$ and **5** in $CD_2Cl_2$ solution showed a number of phosphoramide-bound species, Figure 10. The first resonance appears at $\delta = -118.8$ ppm (t, $J = 15$ Hz), which is within the five-coordinate region of the $^{29}Si$ spectrum, and must be bound by two phosphoramides as seen in the triplet coupling pattern. This signal is assigned to the cationic species [*trans*-$SiCl_3 \cdot \mathbf{5}_2]^+Cl^-$, Scheme 5. The other peaks fall into the six-coordinate regime, of which the two major signals appear at $\delta =$

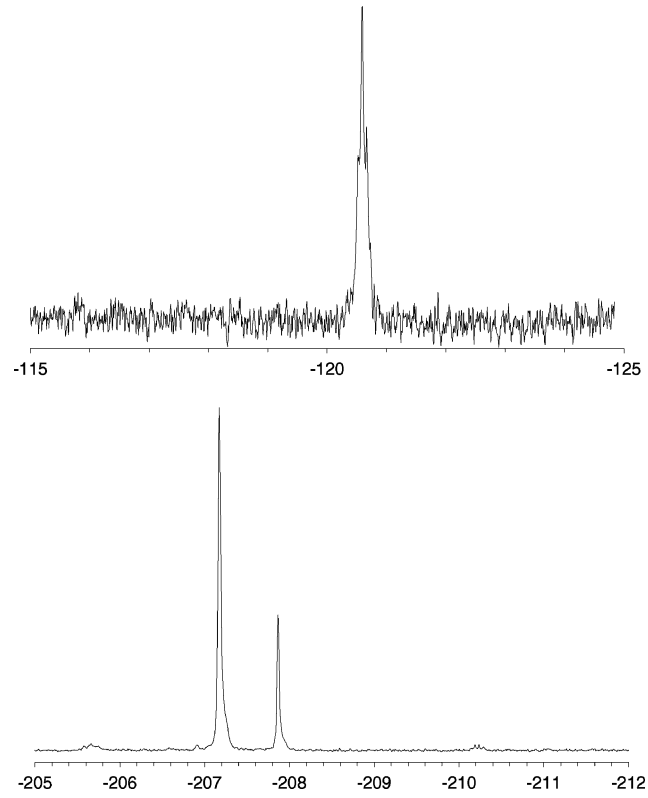


***Figure 9.*** $^{29}Si$ NMR spectra of a mixture of $SiCl_4$ and HMPA in $CD_2Cl_2$ at −70 °C.

−205.5 (t, $J = 15$ Hz) and −207.0 ppm (s) and two broad signals at −205 and −206.5 ppm. The species corresponding to the triplet resonance at −205.5 ppm is definitively doubly ligated, but the coordination environment of species corresponding to the broad singlet at −207.0 ppm is less well-defined. On the basis of the coupling constants, the signal at −205.5 ppm is assigned to the *trans*-$SiCl_4 \cdot \mathbf{5}_2$ complex and that at 207.0 to *cis*-$SiCl_4 \cdot \mathbf{5}_2$. The ill-defined signals are also clearly six-coordinate species and thus could be the trisphosphoramide-bound cations that were identified in our studies with HMPA and $SiCl_4$.

In view of the lack of a nonlinear effect in reactions catalyzed by **5**, the composition of the complexes formed from a nearly racemic mixture of **5** was of interest. The spectra shown in the bottom of the two chemical shift regimes in Figures 10 ($^{29}Si$ NMR) and 11 ($^{31}P$ NMR) display one additional signal each. Thus, both cationic, five-coordinate and neutral, six-coordinate compounds can exist as roughly equal mixtures of homo- and heterochiral complexes.

**4.3. Bisphosphoramide 4c/$SiCl_4$.** $^{29}Si$ NMR spectroscopic analysis of a 2.7:1 mixture of $SiCl_4$ and **4c** in $CD_2Cl_2$ solution also showed three phosphoramide-bound species in addition to free $SiCl_4$ (−19 ppm), Figure 12. All three species appear as triplets and therefore are all coordinated to two phosphorus moieties.[35] The first species ($\delta = -118.4$ ppm (t, $J = 14$ Hz)) falls in a region that is indicative of a five-coordinate silicon complex. Because the coupling constant is nearly identical to that seen in the five-coordinate complex with the monophosphoramide **5** (and is consistent with a trans arrangement of the ligands), the signal is assigned to the dimeric trichlorosilyl

(35) Since the phosphoramide/silicon ratios of these three species are the same, the relative abundances will not change with the concentration of either phosphoramide or silicon.

***Scheme 5***

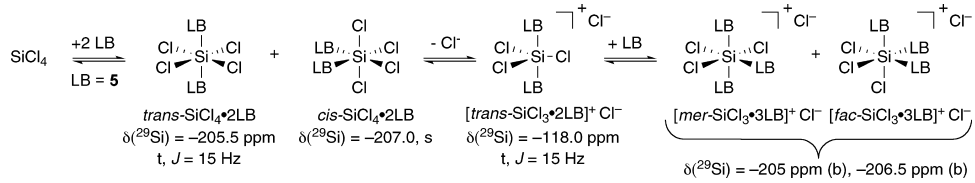


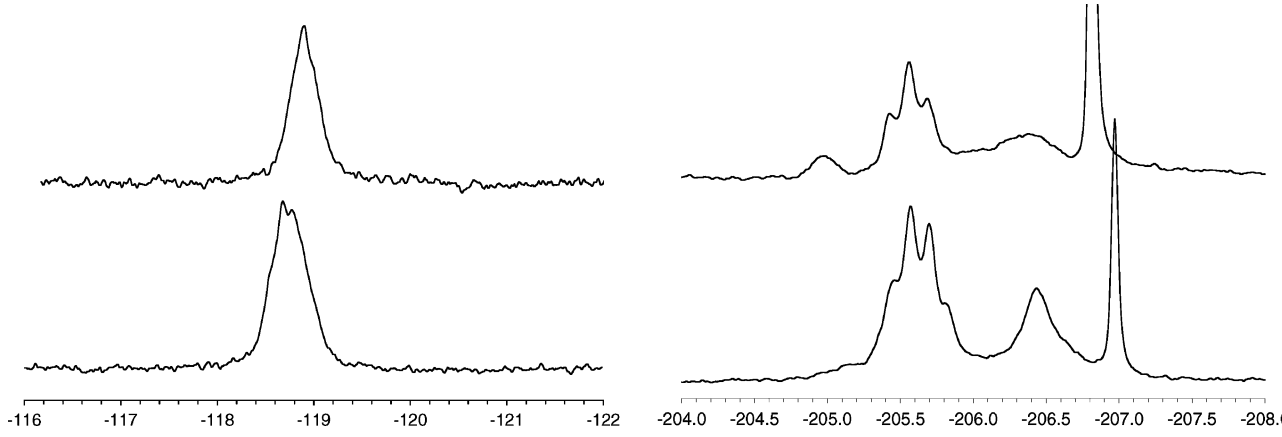


***Figure 10.*** Portions of the $^{29}$Si NMR spectra of $SiCl_4$ and **5** in $CD_2Cl_2$ at −70 °C. (Top) Enantiopure (*R*)-**5**. (Bottom) 54:46 mixture of (*R*)- and (*S*)-**5**, which gave an apparent diastereomer ratio of ca. 1:1.

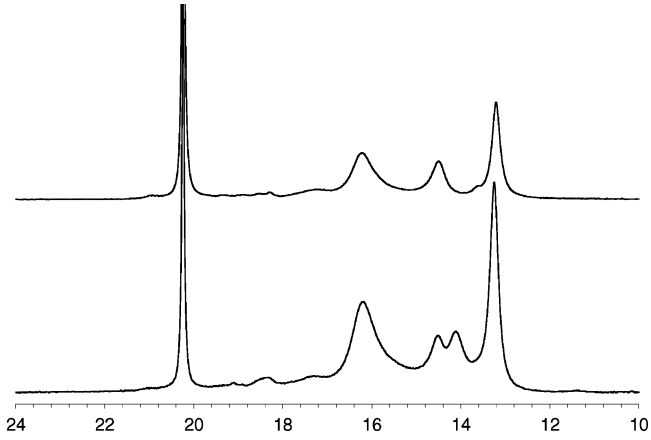


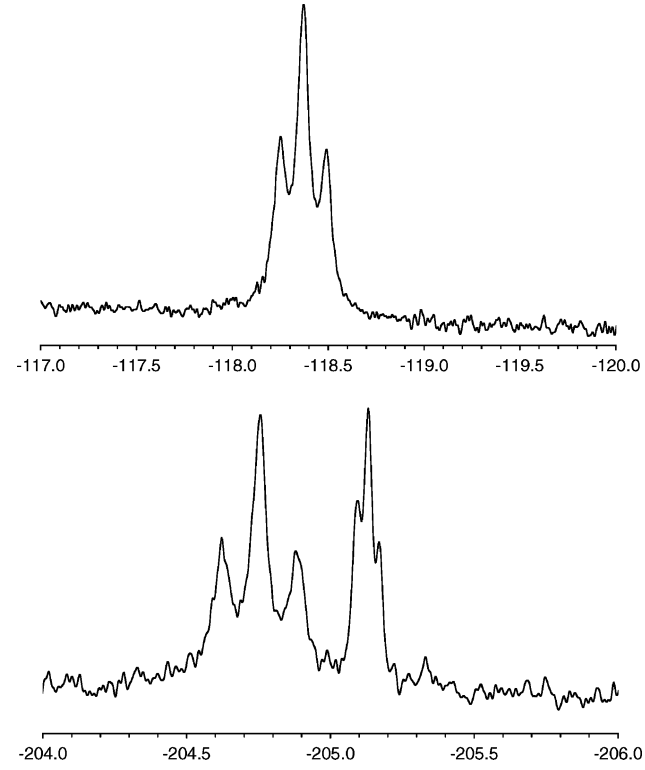


***Figure 11.*** $^{31}$P NMR spectra of $SiCl_4$ and **5** in $CD_2Cl_2$ at −70 °C. (Top) Enantiopure (*R*)-**5**. (Bottom) 54:46 mixture of (*R*)- and (*S*)-**5**, which gave an apparent diastereomer ratio of ca. 1:1.

***Figure 12.*** $^{29}$Si NMR spectra of $SiCl_4$ and **4c** in $CD_2Cl_2$ at −70 °C.

cation, [*trans,trans*-$SiCl_3$·**4c**]$_2^{2+}$2$Cl^-$ (see Figure 14). The other two phosphorus-bound species fall within the six-coordinate regime at $\delta = -204.8$ (t, $J = 15$ Hz) and −205.1 ppm (t, $J =$ 5 Hz). These two species are each bound to two identical phosphorus atoms with different geometrical arrangements around the silicon octahedron.

The $^{31}$P NMR spectrum of this mixture is also informative, Figure 13. First, even at this ratio (2.7 $SiCl_4$/**4c**) only a trace of **4c** is observed, showing the high thermodynamic preference for complexation of the Lewis base. Second, four discrete resonances are visible in the chemical regime of complexed phosphoramides.[31] From these data, four limiting structures for neutral, six-coordinate complexes can be considered, Figure 14. Although the spectroscopic data alone cannot distinguish between monomeric and dimeric complexes, the dimeric complexes would explain the half-order kinetic behavior of **4c** (vide supra). On the basis of the magnitude of the two coupling constants ($^3J_{^{31}P,^{29}Si}$) and the nonequivalent intensities of the two signals, the resonance at −204.9 ppm is assigned to the [*trans,trans*-$SiCl_4$·**4c**]$_2$ complex and the resonance at −205.2 ppm to the [*cis,cis*-$SiCl_4$·**4c**]$_2$ complex (see Figure 14). The mixed dimer [*trans,cis*-$SiCl_4$·**4c**]$_2$ would display equal intensity signals for the two silicon nuclei and can therefore be eliminated. The expected monomeric chelate *cis*-$SiCl_4$·**4c** can be ruled out by the magnitude of the coupling constant. Neutral bis-phosphoramide−$SiCl_4$ complexes display a strong preference to maintain a trans geometry that would disfavor the formation

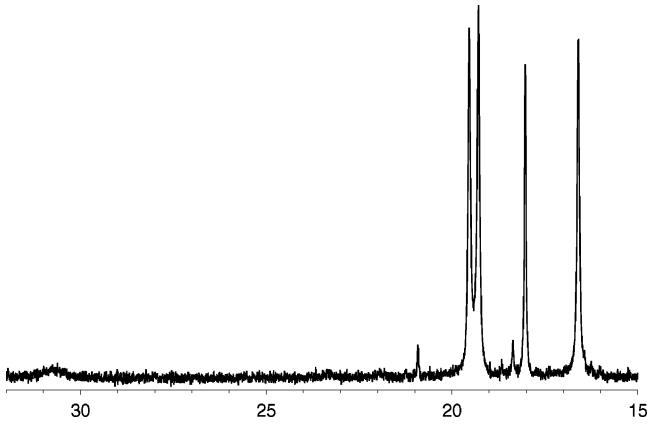


***Figure 13.*** $^{31}$P NMR spectra of $SiCl_4$ and **4c** in $CD_2Cl_2$ at −70 °C.

of *cis*-$SiCl_4$·**4c**. The observation of four $^{31}$P signals is not easily reconciled with the data from the $^{29}$Si spectrum. The dimeric complexes in Figure 14 have nominal $D_3$ symmetry, and thus all the phosphorus nuclei are homotopic. However, we cannot rule out ground state conformations of lower symmetry. Therefore, combining the kinetic data with the spectroscopic observations, all of the silicon species are proposed to be bridged dimers.

The available data cannot eliminate the closely related bridged structure [*trans,trans*·**6**]$^{2+}$2Cl$^-$. This chloride-bridged species also has $D_3$ symmetry and is thus a possible candidate for the resonance at −118.5 ppm. However, the magnitude of the $^3J_{^{31}P-^{29}Si}$ (14 Hz) can rule out any cis-configured complexes of this type as well as the phosphoramide-bridged structure **7**. In addition, **7** is asymmetric, so in the absence of rapid ligand topoisomerization at −70 °C, this species can also be ruled out.

**4.4. Bisphosphoramide 4d/$SiCl_4$.** The $^{29}$Si NMR spectrum of a 3.0:1 mixture of $SiCl_4$ to bisphosphoramide **4d** in $CD_2Cl_2$ solution, Figure 15, looked similar to that from bisphosphoramide **4c** but differed markedly in the ratios of the signals. As before, a strong signal at $\delta = -118.6$ ppm (t, $J = 14$ Hz) revealed the dominant presence of a cationic, five-coordinate complex. Two additional, weak and featureless signals at $\delta = -178$ and −206 ppm suggest the mutual coexistence of neutral, six-coordinate complexes. The splitting patterns of the six-coordinate species were hard to discern. Interestingly, the relative amounts of these species were different for **4d** and **4c**, such that bisphosphoramide **4d** clearly favored a five-coordinate, cationic resting state. Also, for **4d** a single peak is dominant in the $^{31}$P spectrum together with a larger amount of free **4d**, Figure 16. As with **4c**, the structure is assigned to a cyclic, dimeric, five-coordinate cation, [*trans,trans*-$SiCl_3$·**4d**]$_2^+$2Cl$^-$.

**4.5. Bisphosphoramides 4a/$SiCl_4$ and 4b/$SiCl_4$.** The $^{29}$Si spectra of the shorter tethered bisphosphoramides **4a** and **4b** were significantly different compared to those of **4c** and **4d**. The spectra from the $n = 4$ tethered **4b** were of slightly better quality and will be discussed first.

The $^{29}$Si spectra of **4b** in the presence of 3.0 equiv of $SiCl_4$ contained no species in the five-coordinate regime (−115 to −125 ppm), but a signal at $\delta = -185.5$ ppm (t, $J = 2$ Hz)

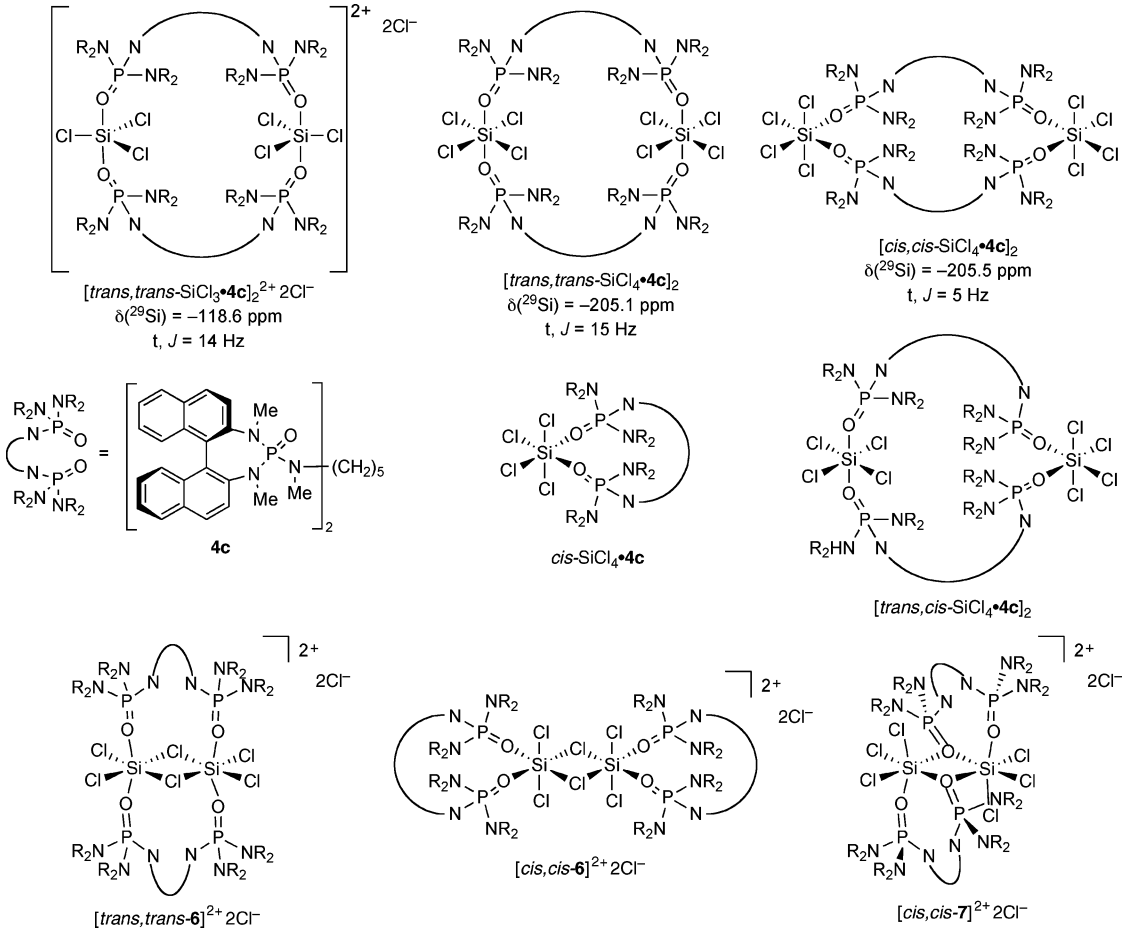


***Figure 14.*** Proposed structures for the complexes of **4c** with $SiCl_4$.

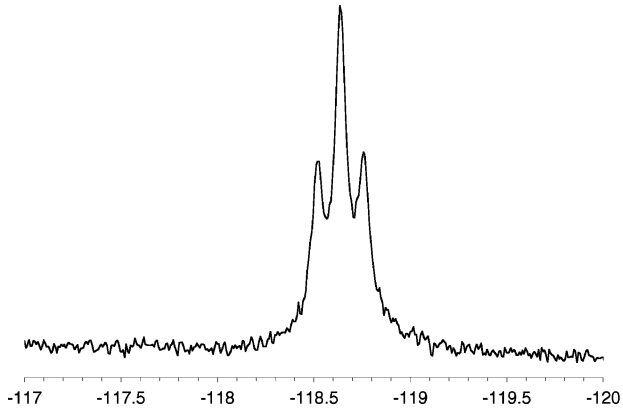


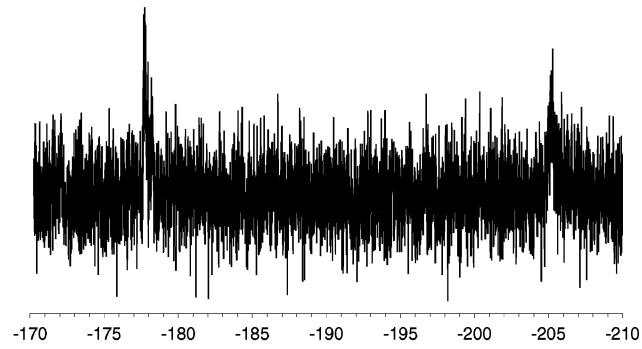


***Figure 15.*** Portions of the $^{29}Si$ NMR spectra of $SiCl_4$ and **4d** in $CD_2Cl_2$ at $-70$ °C.

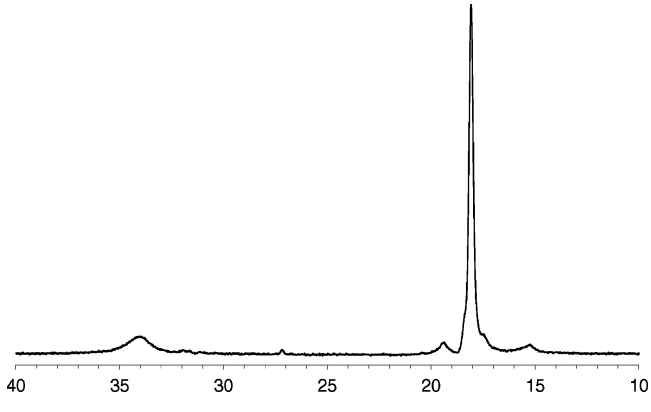


***Figure 16.*** $^{31}P$ NMR spectra of $SiCl_4$ and **4d** in $CD_2Cl_2$ at $-70$ °C.

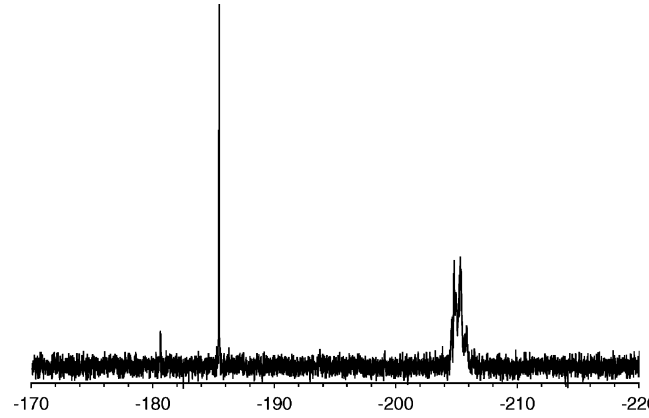


***Figure 17.*** Portions of the $^{29}Si$ NMR spectra of $SiCl_4$ and **4b** in $CD_2Cl_2$ at $-70$ °C.

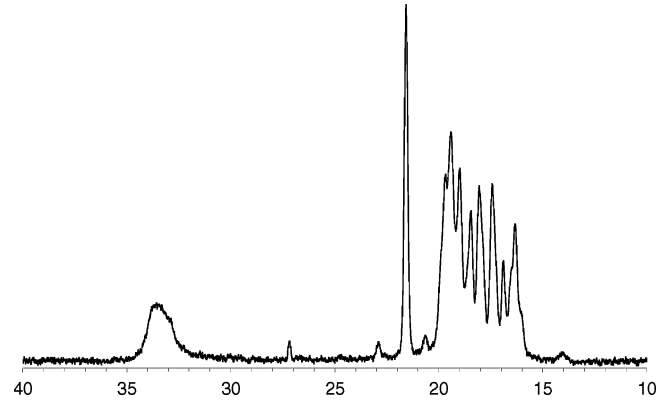


***Figure 18.*** $^{31}P$ NMR spectra of $SiCl_4$ and **4b** in $CD_2Cl_2$ at $-70$ °C.

appeared along with several peaks between $\delta = -204$ and $-206$ ppm, Figure 17. The signal at $\delta = -185.5$ ppm in the $^{29}Si$ spectrum is assigned to the cis-chelated, monomeric, neutral, six-coordinate species *cis*-$SiCl_4$·**4b**. The assignment of the signals in the six-coordinate region is more ambiguous, particularly because their splitting patterns cannot be discerned, but they are tentatively assigned to cyclic dimers [*trans,trans*-$SiCl_4$·**4b**]$_2$ and [*cis,cis*-$SiCl_4$·**4b**]$_2$, similar to those for **4c**. The $^{31}P$ spectrum of **4b** with $SiCl_4$ is very complex, and at this time, assignment of the individual signals to specific structures is not possible, Figure 18 (see Figure 19 for proposed structures).

Catalyst **4a** showed a $^{29}Si$ NMR spectrum similar to that from **4b**: a signal at $\delta = -186.3$ ppm (broad singlet) and two signals between $\delta = -205.4$ and $-206.0$ ppm, Figure 20.[36] The structural assignments are the same as those for **4b**. The broad singlet at $\delta = -186.3$ ppm would likely show a triplet splitting with better resolution. The coupling constant must be smaller than 2 Hz, that of **4b**, which is indicative of a smaller bite angle in the chelated structure. The $^{31}P$ NMR spectrum of this mixture is also too complex to be interpreted, Figure 21.

## Discussion

**1. Brief Summary of Results.** To facilitate the following discussion of the mechanism and catalytic cycles, a brief summary of both the kinetic experiments and resting-state observations would be helpful. The aldol reaction (with catalyst **4c**) displayed first-order dependences on both aldehyde and silyl ketene acetal but zero-order dependence on $SiCl_4$. A small inverse dependence on added chloride ion was noted, but no dependence at all on added triflate ion. No rate dependence on the concentration of added base nor $Cr(dpm)_3$ was noted. Most interesting, however, was the dependence on the catalyst. HMPA showed a two-thirds order, with a slow overall rate and a resting state composed of a cationic 3:1 complex of $[HMPA_3 \cdot SiCl_3]^+Cl^-$ and hexacoordinate neutral 2:1 complexes $[HMPA_2 \cdot SiCl_4]$. The monophosphoramide **5**, also a slow-acting catalyst, displayed a first-order kinetic dependence and a resting state comprising an equilibrium mixture of doubly ligated, cationic, five-coordinate and doubly ligated, neutral, six-coordinate silicon species. Among the tethered bisphosphoramides, **4c**, the catalyst of choice for maximizing enantioselectivity, showed a rapid rate of reaction, with a half-order kinetic dependence. The resting state is comprised of a mixture of two neutral, six-coordinate complexes with each

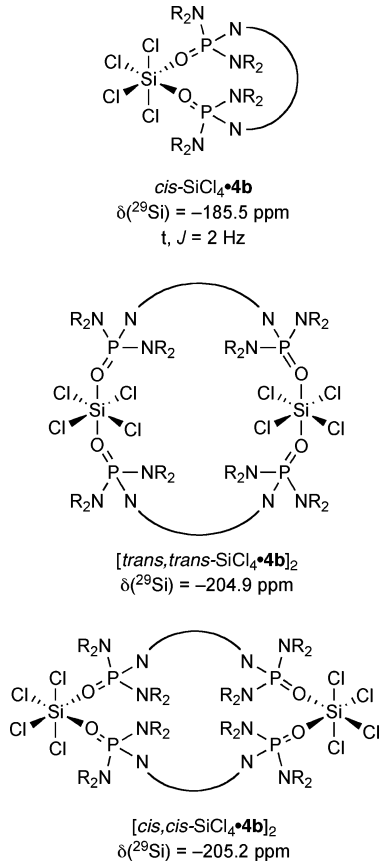


***Figure 19.*** Proposed structures for the complexes of **4b** with $SiCl_4$.

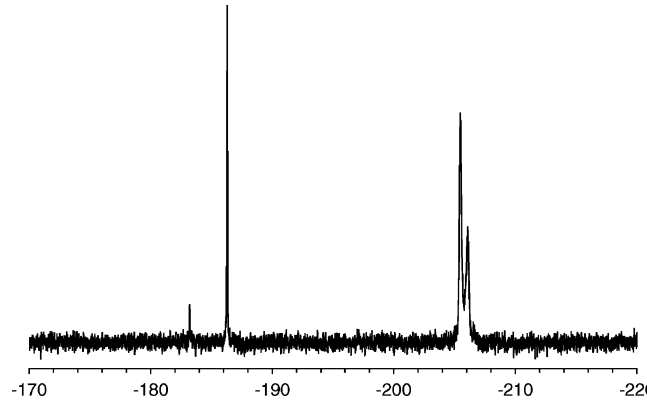


***Figure 20.*** Portions of the $^{29}Si$ NMR spectra of $SiCl_4$ and **4a** in $CD_2Cl_2$ at −70 °C.

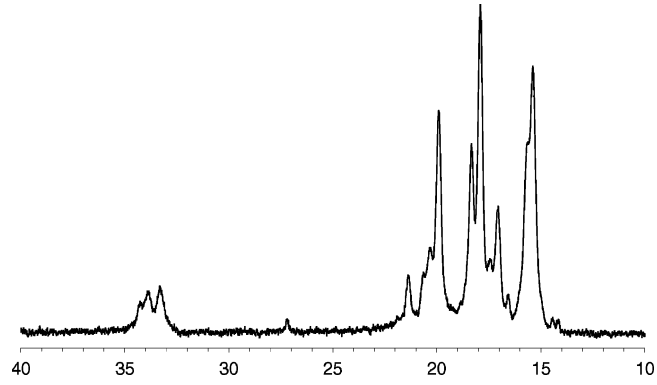


***Figure 21.*** $^{31}P$ NMR spectra of $SiCl_4$ and **4a** in $CD_2Cl_2$ at −70 °C.

silicon center bound to two phosphoramides along with a small amount of the doubly ligated, cationic, five-coordinate species, which is proposed to be the catalytically relevant species. Similarly, **4d** mimics the overall rate and half-order kinetic dependence observed for **4c**, but the doubly ligated, cationic, five-coordinate resting structure predominates. Phosphoramides **4a** and **4b** are the most powerful catalysts, providing much faster overall rates of reaction (albeit with attenuated enantioselectivities) and first-order kinetic dependencies. The resting states are mixtures of monomeric and dimeric neutral, six-coordinate complexes.

**2. Partial Order in Stoichiometric Reactants.** The first-order behavior for both the silyl ketene acetal **1b** and 1-naphthaldehyde is not surprising for a bimolecular reaction and demonstrates that the rate-limiting step is either the aldolization event, a desilylation event, or a catalyst turnover event. While the latter two cannot be ruled out by these data, we believe the aldolization step is turnover-limiting. Both of the post-aldolization steps are believed to be rapid when compared to the aldolization step.[37] Furthermore, it is difficult to imagine a scenario wherein the aldolization could be reversible yet still give such high enantioselectivities.

The insensitivity of the reaction rate to the concentration of $SiCl_4$ (even though this reagent is required in stoichiometric quantities) provides an important insight into the resting structure of the phosphoramide catalyst. Zeroth-order behavior in $SiCl_4$ implies that **4c** is saturated under these conditions, a conclusion supported by the lack of free **4c** in the $^{31}P$ NMR spectrum, Figure 13. Under the initial rate (and preparative reaction) conditions, the concentration of $SiCl_4$ is always much larger than the concentration of the Lewis base. Therefore, since all of the available phosphoramide is bound in some form with $SiCl_4$, the rate of the reaction is dependent not upon the concentration of $SiCl_4$ but instead upon the concentration of the Lewis base, which in turn dictates the concentration of the active, cationic, catalytic complex.

The results of the control experiments were all anticipated. Varying the concentration of diisopropylethylamine or $Cr(dpm)_3$ demonstrates that their addition does not affect the outcome of the reaction. Both had a beneficial effect upon reproducibility, however, as addition of the base prevented the Brønsted acid catalyzed aldol reaction from occurring,[38] while addition of the chromium reagent decreased the relaxation delays required to repeatedly obtain quantitative integration data.

Addition of tetrabutylammonium triflate or chloride was performed to probe the proposed cationic nature of the catalyst. If the catalyst is cationic, the addition of exogenous chloride ions should inhibit the reaction, while the addition of triflate should not affect the rate of reaction. Indeed, the addition of tetrabutylammonium chloride does inhibit the reaction, and this inverse partial order in added chloride supports the cationic nature of the intermediates. The addition of tetrabutylammonium triflate had no effect upon the rate of reaction.

(36) The small signals at $\delta = -180.6$ ppm for **4b** and $\delta = -183.2$ ppm for **4a** are too small to be interpreted but may correspond to conformers of *cis*-$SiCl_4$·**4b** and *cis*-$SiCl_4$·**4a** frozen out at low temperature.

(37) Turnover-limiting desilylation is rarely seen. For a thorough discussion of the consequences of silicon group transfer in Mukaiyama aldol additions, see ref 1b.

**3. Partial Order in Catalysts and Their Resting Structures.** Taken together, these two sets of data, i.e., the kinetic analyses and $^{29}$Si NMR studies of the catalysts, offer the greatest challenges to interpretation but also provide the most insight. One of the most important facts required for a detailed knowledge of a catalytic reaction mechanism is the molecularity of the catalyst in the turnover-limiting transition structure. This knowledge can be obtained by determining the resting state of the catalyst ($N_{GS}$) and the kinetic order in catalyst. The molecularity in the transition structure ($N_{TS}$) is then simply expressed in eq 1.[39]

$$N_{TS} = N_{GS} \times \text{kinetic order} \quad (1)$$

Thus, for the purposes of the following discussion, the general mechanistic scheme shown in Figure 22 applies. In this formulation, the first steps involve the pre-equilibrium activation of $SiCl_4$ by the Lewis base (LB) (Figure 22, eq 1) and the activation of the aldehyde by association with the chiral siliconium complex (Figure 22, eq 2). We posit that the rate-determining and stereodetermining step is the attack of the silyl ketene acetal on the activated aldehyde complex (Figure 22, eq 3), which is followed by a rapid desilylation (Figure 22, eq 4). The catalyst turnover step involves the chelation of the trichlorosilyl moiety to form the spectroscopically observed end product and release the Lewis base catalyst (Figure 22, eq 5). The composition of the reactive complex $[LB_nSiCl_3 \cdot RCHO]^+Cl^-$ is established by (1) first-order kinetic dependence on aldehyde and silyl ketene acetal, (2) zeroth-order kinetic dependence on $SiCl_4$, and (3) $N_{TS}$, the molecularity of LB in the turnover-limiting step. The latter will be established for each catalyst in the following sections.

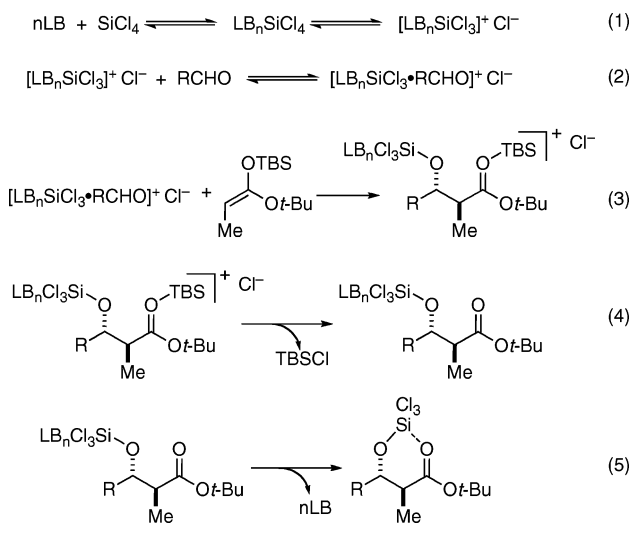


***Figure 22.*** Generalized mechanism for the aldolization process.

**3.1. Monophosphoramide (5) and HMPA.** The mechanism for aldolization catalyzed by **5** is the easiest to explain and aids in understanding the behavior of the other catalysts. The $^{29}$Si NMR spectrum of **5** with $SiCl_4$ reveals that the resting state of the catalyst is comprised of three silicon species (one five-coordinate and two six-coordinate), each with two bound phosphoramides. Because the reaction displays first-order kinetic dependence on the phosphoramide, the transition structure must also contain two molecules of **5**. However, the arrangement of the two ligands in the silicon coordination sphere cannot be deduced from these data. Interestingly, **5** affords a much lower enantioselectivity compared to **4a**−**4c**, suggesting that the additional geometrical and conformational degrees of freedom available to the monomer lead to kinetically competent but sterically less biased catalysts.

The studies with HMPA confirm our understanding of the ground- and transition-state structures for **5**. The existence of a 3:1 HMPA/$SiCl_4$ resting state according to $^{29}$Si NMR and solid-state characterization,[31] combined with the observed two-thirds kinetic order in HMPA, corroborates the notion that the active catalytic species is a cationic, five-coordinate siliconium complex bearing two phosphoramides.

**3.2. Nonlinear Effects.** For a catalytic system in which the resting state possesses two catalyst molecules and still shows first-order kinetic dependence on catalyst (i.e., $N_{TS} = 2$), the absence of nonlinear effects can be interpreted a number of different ways. Because the resting state of the catalytically active species with the monophosphoramide **5** is doubly ligated, the first-order dependence upon phosphoramide can only be explained if two phosphoramides are bound in the transition structure; therefore, a mono-ligated pathway cannot explain the lack of a nonlinear effect. Two limiting scenarios can be formulated: either the heterochiral 2:1 complex [(*R*)-**5**,(*S*)-**5**$\cdot SiCl_3]^+Cl^-$ does not form ($K = 0$), or the hetero- and homochiral complexes [(*R*)-**5**,(*R*)-**5**$\cdot SiCl_3]^+Cl^-$ have identical reactivities ($g = 1$).[29] To determine which of these two possibilities is correct, spectroscopic studies of the resting structure with nearly racemic mixtures of the monophosphoramide were carried out. The $^{29}$Si NMR spectra of these mixtures definitively demonstrate that both the hetero- and homochiral complexes form in solution and are present in nearly equal amounts. Thus, the most reasonable explanation for the lack of a nonlinear effect is that both the homo- and heterochiral complexes have identical reactivities. Inspection of species **8**, **9**, and **10**, Figure 23, illustrates the origin of this behavior. All four complexes contain a phosphoramide moiety situated trans to the bound aldehyde and a second phosphoramide located cis to the bound aldehyde.[40] In this model, the proximal cis-bound phosphoramide is responsible for the orientation of the aldehyde and also controls the topicity of attack on the carbonyl group. The trans-situated phosphoramide is required for reactivity, but it is located too far from the aldehyde to have any effect upon the stereochemical outcome of the reaction. Thus, in the homochiral complexes **8** and *ent*-**8**, the aldehyde is in the same environment and is equally activated as in the corresponding heterochiral complexes **9** and **10**, respectively.

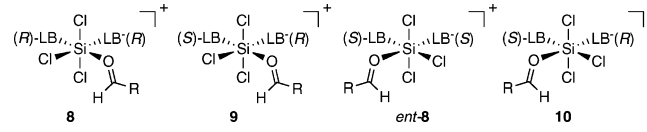


***Figure 23.*** Reactive homo- and heterochiral *mer*-cis complexes of an aldehyde.

**3.3. Bisphosphoramides 4a and 4b.** Three- and four-methylene-linked catalysts **4a** and **4b** share the same kinetic behavior and quite similar $SiCl_4$ complexes, as seen in their $^{29}$Si NMR spectra. Each species observed in the $^{29}$Si spectra

(38) The preparative reactions do not require the addition of an amine base if the $SiCl_4$ is distilled before use. Due to the nature of the RI-NMR device, each sample must be momentarily exposed to the ambient atmosphere, which can be avoided when these reactions are run preparatively. Consequently, we decided to add the base to remove any adventitious acid that may be formed from this exposure.

is six-coordinate, with two bound phosphoramides. Unlike the monomer, the bisphosphoramides can chelate the silicon atom. On the basis of the $^{29}$Si chemical shift and the $^{3}J_{^{31}P,^{29}Si}$, the catalyst ground states are assigned to be cis-chelated, neutral, six-coordinate 1:1 complexes of the bisphosphoramides and $SiCl_4$. The first-order behavior means that this chelated structure is preserved in the transition structure. This observation provides further evidence that two phosphoramides are bound to silicon in the turnover-limiting transition structure.

**3.4. Bisphosphoramides 4c and 4d.** Five- and six-methylene-linked catalysts **4c** and **4d** behave the same way and can be discussed together. Unlike the shorter-chained ligands **4a** and **4b**, these phosphoramides prefer to form a five-coordinate, doubly ligated, cationic species with $SiCl_4$. The half-order kinetic behavior observed for **4c** and **4d** strongly suggests that a dimeric resting state undergoes a dissociation leading to a monomeric reactive complex with the aldehyde; i.e., the ground-state structure contains two bisphosphoramide·$SiCl_3$ units, and the transition structure contains one. The simplest way to accommodate this mathematical mandate is to propose that the resting-state structures are cyclic dimers, which break apart to give two equivalent active species. From the $^{29}$Si NMR spectra, both neutral, six-coordinate complexes, [*trans,trans*-$SiCl_4$·**4c**]$_2$ and [*cis,cis*-$SiCl_4$·**4c**]$_2$, are present but only one cationic, five-coordinate complex, [*trans,trans*-$SiCl_3$·**4c**]$_2^{2+}2Cl^-$. It is this latter species that is believed to undergo reversible binding of the aldehyde and dissociation to a reactive monomeric complex, vide infra.

The analysis of **4d** follows along similar lines. Of special note is the relative simplicity of the $^{29}$Si and $^{31}$P spectra for **4d**, where essentially only one major five-coordinate cationic complex, [*trans,trans*-$SiCl_3$·**4d**]$_2^{2+}2Cl^-$, is observed. Because **4d** shows a half-order kinetic dependence, it is proposed that this species must be dimeric.

**3.5. Derivation of the Rate Equation for Aldolizations.** Given the knowledge of the resting states and the partial orders in the various catalysts (as well as the orders in **1b**, **2b**, $SiCl_4$, and $n$-$Bu_4N^+Cl^-$), it should be possible to derive a kinetic equation under the assumption of the general mechanistic scheme shown in Figure 22. Two derivations are needed, one for a monomeric resting state (for catalysts **4a** and **4b**) and one for a dimeric resting state (**4c** and **4d**).[41]

For catalysts **4a** and **4b** the relevant pre-equilibria, mass balance, and rate expressions are shown in Figure 24. Rearranging all of the equilibrium expressions in terms of [C$^+$], solving for [C$^+$], and substituting that expression in the rate equation gives eq 2. This equation reduces to eq 3 for low concentration of chloride, i.e., little ionization, which was spectroscopically confirmed (no species between $\delta = -115$ and $-125$ ppm). Equation 3 fits the experimental observation of first-order behavior in the catalysts.

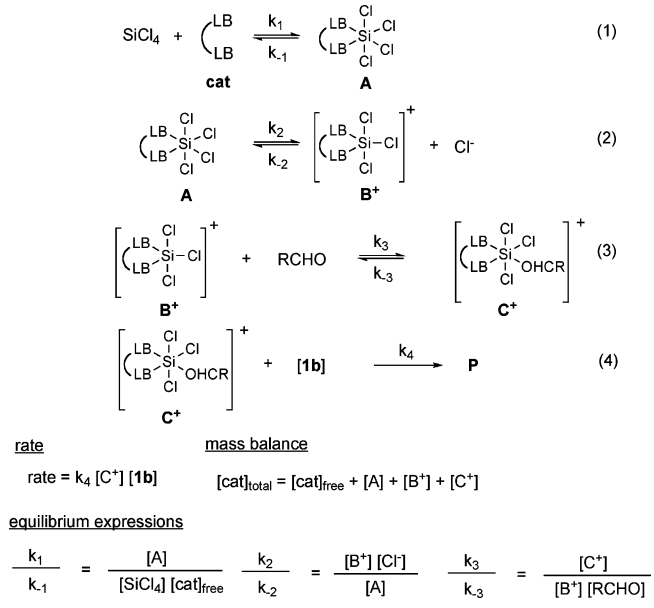


***Figure 24.*** Derivation of kinetic expression for a monomeric catalyst resting state, **4a** and **4b**.

$$\text{rate} = k_1k_2k_3k_4[SiCl_4][RCHO][\mathbf{1b}][cat]_{total}/\{k_{-1}k_{-2}k_{-3}[Cl^-] + k_1k_{-2}k_{-3}[Cl^-][SiCl_4] + k_1k_2k_{-3}[SiCl_4] + k_1k_2k_3[SiCl_4][RCHO]\} \quad (2)$$

For very small [Cl$^-$], eq 2 simplifies to

$$\text{rate} = \frac{k_1k_2k_3k_4[RCHO][\mathbf{1b}][cat]_{total}}{k_1k_2k_{-3} + k_1k_2k_3k_4[RCHO]} \quad (3)$$

For catalysts **4c** and **4d** the relevant pre-equilibria, mass balance, and rate expressions are shown in Figure 25. Solving the equation for $[cat]_{total}$ gives a complex, five-term expression that can be simplified by making some reasonable assumptions: (1) the term $[cat]_{free}$ can be ignored because no free catalyst **4c** or **4d** is ever observed in the $^{31}$P NMR spectra, and (2) the terms [**C**$^+$] and [**D**$^+$] can be ignored because these species are never detected in the $^{29}$Si NMR spectra or during the analysis of reactions.

From there, three equations can be derived by assuming that different species are the dominant contributors to the catalyst resting state: (1) the resting state is a dimeric, neutral hexacoordinate species **A**, (2) the resting state is a dimeric, cationic pentacoordinate species **B**$^{2+}$, or (3) the resting state is a combination of **A** and **B**$^{2+}$. Under assumption (1) the expression reduces to eq 4, which fits the partial order dependencies on **1b**, **2b**, catalysts (**4c** and **4d**), and chloride, except that chloride is integral inverse order. Under assumption (2) the expression reduces to eq 3, which fits the partial order dependencies on **1b**, **2b**, and catalysts (**4c** and **4d**) and but shows no dependence on chloride. This result makes sense if the resting state is already ionized. Under assumption (3) the expression reduces to eq 6, which fits the partial order dependencies on **1b**, **2b**, and catalysts (**4c** and **4d**) and unifies the two previous scenarios for the chloride dependence. Thus, if $k_{-2}/k_2$ is large (i.e., a neutral, dimeric resting state), then eq 6 reduces to eq 4, which predicts

(39) Collum, D. B.; McNeil, A. J.; Ramirez, A. *Angew. Chem., Int. Ed.* **2007**, *46*, 3002–3017.

(40) For octahedral $LB_2SiCl_3$·RCHO complexes, three constitutional isomers exist, two cis (*fac* and *mer*) and one trans. Moreover, each isomer can exist in many conformations that orient the aldehyde differently with respect to the LB groups. Previous computational studies revealed two important features that lead to our formulation of the preferred *mer*-cis isomers shown in Figure 23: (1) the binding of the aldehyde is more favorable in a trans position to an LB group than to a Cl and (2) chlorines prefer to be trans if possible.

(41) See Supporting Information for the full derivation of the kinetic equations.

(42) The influence of ligand structure on the enantioselectivity will also not be discussed herein. For a substantive analysis of enantioselectivity, a detailed understanding of the conformations of the various reactive complexes is required, which will require extensive computational modeling beyond the scope of the present mechanistic study. Although the composition of the various species is now well in hand, their stereochemical attributes are not discernable.

inverse first order in chloride. However, if $k_{-2}/k_2$ is small (i.e., a cationic, dimeric resting state), then eq 6 reduces to eq 5, which predicts no dependence on chloride. The observed −0.2 order in chloride must mean that both cationic and neutral species are present in the resting state (as detected by $^{29}$Si NMR) and are both contributing to the formation of the active monomeric species.

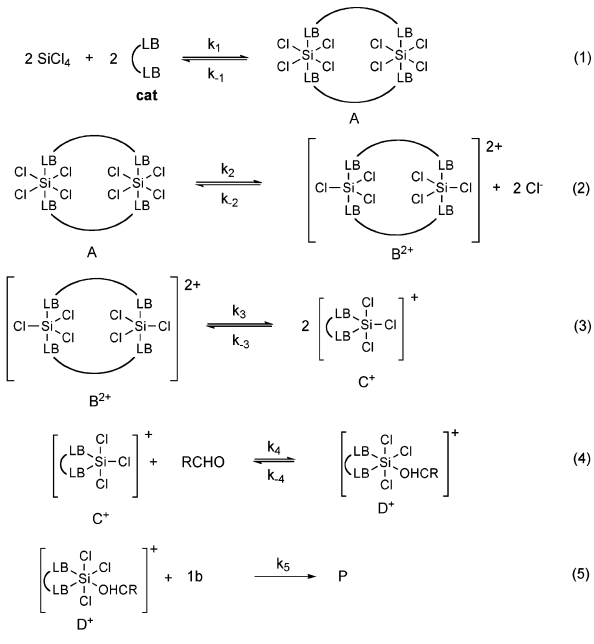


***Figure 25.*** Derivation of kinetic expression for a dimeric catalyst resting state, **4c** and **4d**.

$$\text{rate} = k_5\left(\frac{k_2k_3}{2k_{-2}k_{-3}}\right)^{1/2}\left(\frac{k_4}{k_{-4}}\right)[\text{RCHO}][\mathbf{1b}][\text{cat}]_{\text{total}}{}^{1/2}[\text{Cl}^-]^{-1} \quad (4)$$

$$\text{rate} = k_5\left(\frac{k_3}{2k_{-3}}\right)^{1/2}\left(\frac{k_4}{k_{-4}}\right)[\text{RCHO}][\mathbf{1b}][\text{cat}]_{\text{total}}{}^{1/2} \quad (5)$$

$$\text{rate} = k_5\left(\frac{k_3}{2k_{-3}}\right)^{1/2}\left(\frac{k_4}{k_{-4}}\right)\frac{[\text{RCHO}][\mathbf{1b}][\text{cat}]_{\text{total}}{}^{1/2}}{\left(\frac{k_{-2}}{k_2}[\text{Cl}^-]^2 + 1\right)^{1/2}} \quad (6)$$

**4. Analysis of Differences in Rates for Catalysts 4a−4d and 5. 4.1. Postulate of a Common Catalytic Intermediate.** On the basis of all of the preceding discussion, a catalytic cycle that represents the behavior of all of the catalysts studied herein can be formulated, Figure 26. To facilitate discussion of the factors that influence the differences in rates for the various catalyst structures, it is instructive first to focus on the common features of the catalytic cycles that are believed to be operative for all. The fundamental tenet of the mechanistic hypothesis is that the reactive catalytic species is a cationic, five-coordinate complex bearing two Lewis basic phosphoryl groups, **i**, Figure 26. This species can be formed by dissociation of a chloride ion induced by the Lewis basic ligands, the manner of which is ligand dependent and will be discussed in detail below along

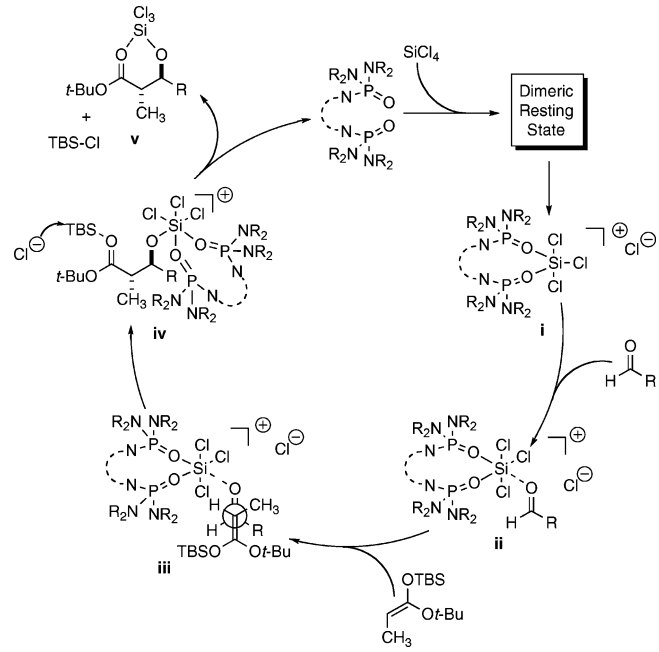


***Figure 26.*** Generalized catalytic cycle for aldolization catalyzed by LB·$SiCl_4$.

with the rationale for identifying complex **i** as the active catalyst. Coordination of **i** by the aldehyde through the oxygen lone pair forms the reactive complex **ii**. This species may also be formed directly from the dimeric resting states through binding of the aldehyde, thus bypassing intermediate **i**. According to the rate equation, the turnover-limiting (and stereodetermining) step is the bimolecular collision between complex **ii** and the silyl ketene acetal via transition structures approximated by depiction **iii**. The origin of the high anti diastereoselectivity has been discussed in detail previously and will not be elaborated further here.[42] The kinetically generated aldolate complex **iv** then undergoes a rapid desilylation to form TBSCl, giving the spectroscopically observable aldolate product **v**. We suspect that the aldolate product is internally coordinated by the ester oxygen, which may play a supporting role in facilitating the catalyst turnover step. The Lewis acidity of the silicon atom in **iv** is certainly less than that in $SiCl_4$, which is critical to allow the Lewis base to dissociate at the end of the cycle. However, the chelation of the $SiCl_3$ subunit would further facilitate the dissociation of the Lewis base for re-entry into the catalytic cycle.[43]

From the rate equation and the foregoing discussion, it is clear that the rate of the aldolization is dependent on the concentration of the reactive complex **ii**.[44] Since the aldehyde is consistent throughout, the concentration of **ii** is related to the pre-equilibria established by the interaction of the phosphoramides with $SiCl_4$ and their affinity for the aldehyde (eqs 2 and 3 in Figure 22). The zeroth-order kinetic dependence of the rate on [$SiCl_4$] implies that, under the reaction conditions (>50:1, $SiCl_4$/ligand), all of the available phosphoramide is coordinated with $SiCl_4$ in some form. Indeed, even under the conditions of $^{31}$P NMR observation (ca. 4:1, $SiCl_4$/ligand), little if any free phosphoramide was detected. The relevant complexes formed in these equilibria, as demonstrated by NMR spectroscopic

(43) Nevertheless, we did observe significant curvature of the kinetic plots beyond 30% conversion, which most likely is ascribed to sequestering of the catalyst by the product aldolate, **v**.

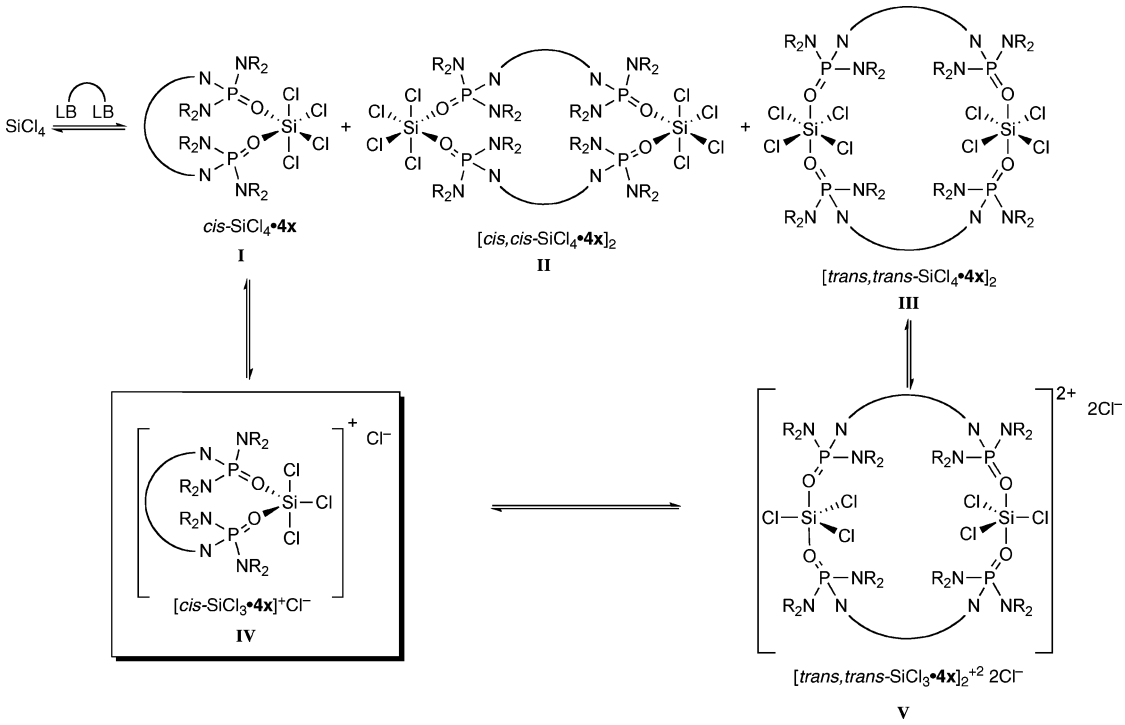


***Figure 27.*** Composition of complexes in bisphosphoramide/$SiCl_4$ pre-equilibria.

***Scheme 6***

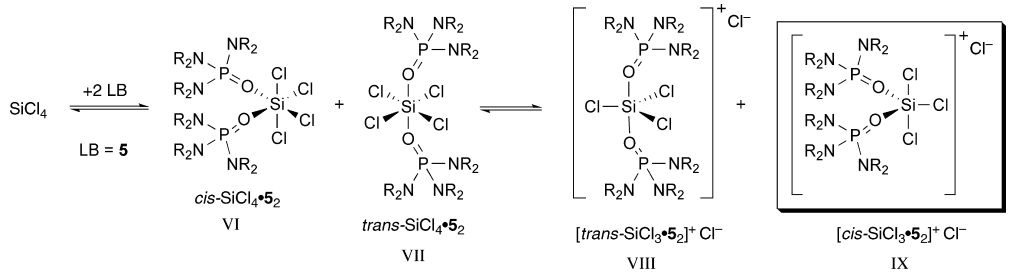


analysis of the mixtures of the bisphosphoramides **4** and $SiCl_4$, are shown in Figure 27. Although the composition of the mixtures could not be rigorously quantified, the general trends can be summarized as follows: (1) **4a** consists of a roughly equal mixture of **I**, **II**, and **III**; (2) **4b** consists primarily of species **II** and **III** along with other neutral, six-coordinate complexes and a lesser amount of **I**; (3) **4c** consists of a roughly equal mixture of **II**, **III**, and **V**; and (4) **4d** consists of a similar mixture of complexes, but more strongly favoring the five-coordinate cation **V** compared to **4c**. Thus, two families of bisphosphoramides can be identified: (1) short tethered ligands that form both monomeric and dimeric, neutral, six-coordinate complexes but do not form cationic, five-coordinate complexes in detectable concentration and (2) longer tethered ligands that form only dimeric complexes of both cationic, five-coordinate and neutral, six-coordinate structures. In no case is the monomeric, cis-five-coordinate cationic complex **IV** detected.

A similar collection of complexes representing the pre-equilibrium of monophosphoramide **5** with $SiCl_4$ is shown in Scheme 6. By NMR analysis, the mixture consists of a roughly equal composition of **VI**, **VII**, and **VIII**. Here again, the cis-five-coordinate cationic complex **IX** is not detected in the $^{29}Si$ NMR spectrum.

To construct a self-consistent hypothesis for the different catalytic activity of the various phosphoramides, one critical assumption must be posited, namely that the cis-cationic complexes of the type **ii**, Figure 26, are the kinetically most competent for activation of the aldehyde toward nucleophilic attack. This assumption is supported by three important lines of evidence. First, the half-order kinetic dependence of reactions in which the catalyst resting state is a dimer, even a cationic dimer such as **V**, Figure 25, suggests that the dimeric species are not kinetically competent and must dissociate to effect the activation of the aldehyde. Second, even monomeric, trans-cationic complexes such as **VIII**, though spectroscopically detectable, are associated with the slowest of the aldolization processes (i.e., catalysis by **5** and HMPA). Third, previous calculations of the various complexes of aldehydes with $[SiCl_3 \cdot \mathbf{4c}]^+$ and ketones with enoxydichlorosilyl·bis(*N*-oxide) cations[1b,13a] showed that electrophilic activation of the aldehyde is strongest in such cationic, octahedral complexes when the

(44) Of course, the rate of the aldolization also depends on the intrinsic reactivity of the different complexes. This feature is impossible to determine without extensive computational study. However, assuming that a cis-chelated cationic complex such as **i** is equally reactive for all phosphoramides **4a**−**4c** and **5** allows us to formulate an intriguing hypothesis about the impact of the different ground states on the overall reaction rates. In-depth computational analyses will be reported in due course.

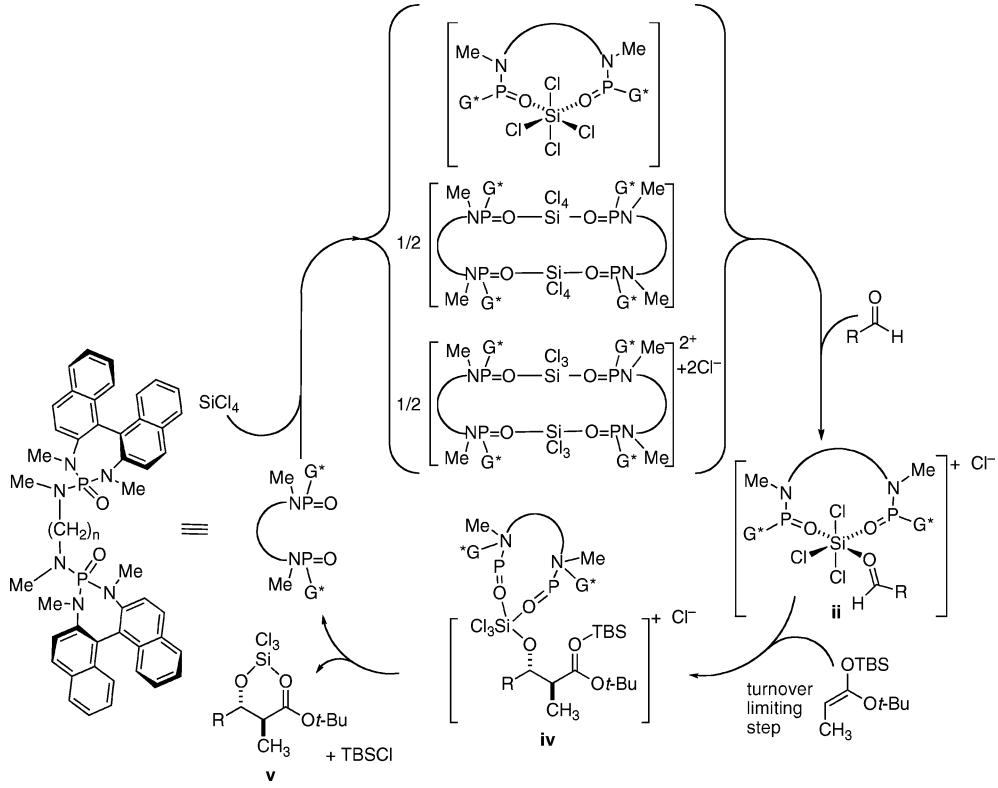

***Figure 28.*** Grand unified catalytic cycle.

carbonyl oxygen is bound through an sp-type orbital, trans to a ligand oxygen. The high s-character of this orbital is a consequence of the polarization of p-character toward the chlorine atoms.[45]

Combining the results from the kinetic analyses, spectroscopic studies, and the postulate of **ii** as a common reactive intermediate, an explanation for the differential reactivity of the phosphoramides can be formulated, Figure 28. Implicit in this analysis is a corollary of the Hammond postulate,[46] which states that species that are close in structure are also close in energy; therefore, the greater the structural reorganization needed to change a resting state to a reactive complex, the greater the energy of that reorganization, and therefore the less favorable is that process.

The composition of the ground-state complexes is dictated by the structure of the bisphosphoramide according to the trends described above. Thus, the shortest tethered bisphosphoramide, **4a** ($n = 3$), forms a substantial amount of the neutral, cis-six-coordinate complex **I**. Because of the first-order kinetic dependence on [**4a**], it is assumed that one molecule of **4a** is also present in the turnover-limiting transition structure. Moreover, the conversion of **I** to **ii** (or its cationic, cis-five-coordinate precursor) represents a minimal structural change and is therefore the most energetically favorable for the various intermediate complexes. Accordingly, reactions catalyzed by **4a** are found to be the fastest. A very similar analysis holds for the next bisphosphoramide, **4b** ($n = 4$), which also shows first-order kinetic dependence on [**4b**] and is the second fastest acting catalyst.

The ground-state composition of the most enantioselective catalyst **4c** ($n = 5$) is a ternary mixture of neutral and cationic dimers **II**, **III**, and **V**. The half-order kinetic dependence requires that the dimers must dissociate to form the reactive intermediate **ii**. Since dimeric, cationic, five-coordinate complex [*trans,trans*-$SiCl_3$·**4c**]$_2^{2+}2Cl^-$ is present in high concentration, it is reasonable to propose that this species is the immediate precursor to **ii** on the basis of the Hammond postulate. Nevertheless, a more significant structural reorganization is needed compared to catalysts **4a** and **4b**, and, indeed, **4c** is a considerably slower acting catalyst. The same analysis holds for the last bisphosphoramide, **4d** ($n = 6$), except that the resting-state composition appears to have a greater proportion of the dimeric, cationic, five-coordinate species [*trans,trans*-$SiCl_3$·**4d**]. Remarkably, this is the slowest acting of the bisphosphoramides, yet it contains the greatest amount of a cationic, five-coordinate species. This highly counterintuitive observation provides strong support for the notion that the trans-coordinated complexes are not kinetically competent.

Finally, the behavior of the monophosphoramide **5** is confluent with the foregoing analysis. The composition of the ground-state complexes with **5** is very similar to the ground-state composition obtained with bisphosphoramide **4c**; namely, they are dominated by 2:1 complexes of both cationic, five-coordinate and neutral, six-coordinate structures. The first-order kinetic dependence on [**5**] implies that two molecules of the phosphoramide are present in the turnover-limiting transition structure. However, this is by far the slowest acting catalyst, which forces the conclusion that even

(45) (a) Curnow, O. J. *J. Chem. Educ.* **1998**, *75*, 910–915. (b) Tandura, S. N.; Voronkov, M. G.; Alekseev, N. V. *Top. Curr. Chem.* **1986**, *113*, 99–189. (c) Bent, H. A. *Chem. Rev.* **1961**, *61*, 275–311.

(46) Hammond, G. S. *J. Am. Chem. Soc.* **1955**, *77*, 334–338.

(47) Magnetization transfer experiments with the HMPA·$SiCl_3^+$ complexes[32] showed rapid reorganization of the ligands without dissociation. Thus, we conclude that the [*cis*-$SiCl_3$·$\mathbf{5}_2$]$^+Cl^-$ complex is kinetically accessible but thermodynamically highly unfavorable.

a simple trans→cis isomerization of [*trans*-$SiCl_3$·**5**$_2$]$^+Cl^-$ to a structure related to [*cis*-$SiCl_3$·**5**$_2$]$^+Cl^-$ (**IX**) is energetically unfavorable, most probably because of steric repulsion.[47] This conclusion is easily reconciled by the different steric consequences of the reorganization of [*trans,trans*-$SiCl_3$·**4c**]$_2^{2+}2Cl^-$ (**V**) to [*cis*-$SiCl_3$·**4c**]$^+Cl^-$ (**IV**) compared to the change from [*trans*-$SiCl_3$·**5**$_2$]$^+Cl^-$ (**VIII**) to [*cis*-$SiCl_3$·**5**$_2$]$^+Cl^-$ (**IX**). The tethered bisphosphoramide has already accommodated the steric energy of cis coordination in its structure, whereas the monophosphoramides must overcome the energetic cost of cis coordination of extremely bulky ligands about the octahedral silicon center.

## Conclusions and Outlook

The origin of the ability of chiral phosphoramides to enhance the Lewis acidity of silicon tetrachloride has been investigated in the context of enantioselective catalysis of Mukaiyama-type aldol addition reactions. The empirical development of bisphosphoramides was guided by the knowledge that two Lewis basic moieties are needed to facilitate ionization of a chloride ion to create the trichlorosiliconium ion that acts as the catalytic species. However, the kinetic behavior of the different bisphosphoramides (that vary the length of the connecting tether) was unknown. By careful kinetic analysis of the aldolizations through the use of rapid injection NMR spectroscopic analysis, a striking difference in the catalytic activity and kinetic order of the bisphosphoramides was revealed. From these kinetic studies, in combination with natural abundance $^{29}Si$ NMR studies of the resting states of the catalytic species, a clear trend emerged that allowed the interpretation of the different kinetic orders. By postulating a common catalytic intermediate comprised of a chelated, trichlorosiliconium ion, the relative rates and kinetic orders of all five catalysts could be understood.

With a clearer understanding of the underpinnings of the process, it is now possible to approach the much more difficult challenge of rationalizing the origins of variable enantioselectivity for the different catalysts. These studies necessarily will require extensive computational modeling and are in progress.

The explosive growth of the field of asymmetric catalysis has yielded spectacular advances in the introduction and development of new, selective chemical reactions. During a time of rapid expansion, the lure of harvesting the most readily accessible results (low hanging fruit) is understandable and can be seen in all corners of the discipline: transition metal, Brønsted acid and base, and especially organocatalysis. However, the most valuable bounty to be extracted from these enterprises is the much harder won insight that comes from a fundamental understanding of the origins of catalysis and selectivity. The lessons gleaned from these investigations contribute to the foundations of organic chemistry that will endure long after the *en vogue* infatuations are replaced by the next fad *du jour*.

**Acknowledgment.** We are grateful for generous financial support from the National Science Foundation (NSF CHE 0414440 and CHE 0717989). M.D.E. thanks Glaxo-Smith Kline for a postdoctoral fellowship.

**Supporting Information Available:** Experimental details for the preparative experiments, general description of the kinetic experiments, all spectroscopic and kinetic data, and kinetic derivations. This material is available free of charge via the Internet at http://pubs.acs.org.

JA902474J